Title

A mechanism for differential sorting of the planar cell polarity proteins Frizzled6 and Vangl2 at the trans-Golgi network

Journal

Journal of Biological Chemistry, 293(22)

ISSN

0021-9258

Authors

Ma, Tianji

Li, Baiying

Wang, Ryan

et al.

Publication Date

2018-06-01

DOI

10.1074/jbc.ra118.001906

A mechanism for differential sorting of the planar cell polarity proteins Frizzled6 and Vangl2 at the *trans*-Golgi network

Received for publication, January 17, 2018, and in revised form, March 12, 2018 Published, Papers in Press, April 17, 2018, DOI 10.1074/jbc.RA118.001906

Tianji Ma[‡], **Baiying Li**[§], **Ryan Wang**[¶1], **Pik Ki Lau**[‡], **Yan Huang**[‡], **Liwen Jiang**[§2], **Randy Schekman**[¶3], and **Yusong Guo**[‡4]

From the [‡]*Division of Life Science, Hong Kong University of Science and Technology, Clear Water Bay, Kowloon, Hong Kong, China, the* [¶]*Department of Molecular and Cell Biology, University of California, Berkeley, California 94720 , and the* [§]*Centre for Cell and Developmental Biology, State Key Laboratory of Agrobiotechnology, School of Life Sciences, Chinese University of Hong Kong, Shatin, New Territories, Hong Kong, China*

Edited by Peter Cresswell

In planar cell polarity (PCP), the epithelial cells are polarized along the plane of the cell surface perpendicular to the classical apical–basal axis, a process mediated by several conserved signaling receptors. Two PCP-signaling proteins, VANGL planar cell polarity protein 2 (Vangl2) and Frizzled6 (Fzd6), are located asymmetrically on opposite boundaries of the cell. Examining sorting of these two proteins at the *trans*-Golgi network (TGN), we demonstrated previously that the GTP-binding protein ADP-ribosylation factor–related protein 1 (Arfrp1) and the clathrin-associated adaptor protein complex 1 (AP-1) are required for Vangl2 transport from the TGN. In contrast, TGN export of Frizzled6 does not depend on Arfrp1 or AP-1. Here, to further investigate the TGN sorting process in mammalian cells, we reconstituted release of Vangl2 and Frizzled6 from the TGN into vesicles *in vitro*. Immunoblotting of released vesicles indicated that Vangl2 and Frizzled6 exit the TGN in separate compartments. Knockdown analysis revealed that a clathrin adaptor, epsinR, regulates TGN export of Frizzled6 but not of Vangl2. Protein interaction analysis suggested that epsinR forms a stable complex with clathrin and that this complex interacts with a conserved polybasic motif in the Frizzled6 cytosolic domain to package Frizzled6 into transport vesicles. Moreover, we found that Frizzled6–epsinR binding dissociates epsinR from AP-1, which may separate these two cargo adaptors from each other to perform distinct cargo-sorting functions. Our results suggest that Vangl2 and Frizzled6 are packaged into separate vesicles that are regulated by different clathrin adaptors at the TGN, which may contribute to their asymmetric localizations.

This work was supported in part by Hong Kong Research Grants Council Grants 26100315, 16101116, and AoE/M-05/12 (to Y. G.). The authors declare that they have no conflicts of interest with the contents of this article.

This article contains Figs. S1–S4.

[1] Present address: Feinberg School of Medicine, Northwestern University, Chicago, IL.

[2] Supported by Hong Kong Research Grants Council Grants CUHK2/CRF/11G, C4011–14R, C4012–16E, and AoE/M-05/12.

[3] Investigator of the Howard Hughes Medical Institute and a Senior Fellow of the Miller Institute, University of California, Berkeley.

[4] To whom correspondence should be addressed. Tel.: 852-34692492; E-mail: guoyusong@ust.hk.

Epithelial tissues are polarized along the apical–basal axis such that the apical plasma membrane and the basolateral plasma membrane are enriched with distinct groups of proteins to perform different physiological functions. In addition to the apical–basal polarity, many epithelial tissues are polarized along the tissue plane on an axis perpendicular to the classical apical–basal axis, a phenomenon referred to as planar cell polarity (PCP).[5] The establishment of PCP is regulated by an evolutionarily conserved set of signaling molecules such as Vangl2 and Frizzled6 (Fzd6) (1). Vangl2 is essential for neural tube closure, cardiac development, and orientation of stereociliary bundles in the cochlea (2–5). Fzd6 controls hair patterning in the skin and regulates nail and claw formation (6, 7). Double knockout of Fzd3 and Fzd6 in mice causes severe defects in neural tube closure and planar polarity of inner-ear sensory hair cells (8).

During PCP signaling, Vangl2 and Frizzleds are asymmetrically localized on opposing cell boundaries (1). The asymmetrically localized PCP proteins are proposed to recruit distinct downstream effectors to drive PCP-mediated processes (9). The mechanisms mediating this asymmetric distribution are poorly understood. One view is that the PCP asymmetry is regulated by intercellular interactions between PCP proteins across cellular boundaries (1, 10). Additional signaling pathways, including the Wg/Wnt4 pathway and the Dachsous/Fat/Four-jointed pathway, are proposed to provide long-range directional information for establishing the PCP asymmetry (11, 12). Besides these, evidence from live imaging analysis demonstrates that vesicles containing Frizzled and vesicles containing Dishevelled, another PCP protein, are preferentially transported to the distal boundaries in *Drosophila* wing (13, 14), suggesting that polarized intracellular trafficking contributes to establishing PCP asymmetry. Although PCP and apical–basal polarity are controlled by distinct molecular mechanisms,

[5] The abbreviations used are: PCP, planar cell polarity; Fzd6, Frizzled6; ER, endoplasmic reticulum; TGN, *trans*-Golgi network; AP-1, adaptor complex 1; GMPPNP, 5′-guanylyl imidodiphosphate; endo H, endoglycosidase H; CHC, clathrin heavy chain; PNG-F, peptide:*N*-glycosidase F; CCV, clathrin-coated vesicle; Ldl2, lethal giant larvae 2; aa, amino acid; siRNA, small interfering RNA; GST, glutathione *S*-transferase; SNARE, soluble *N*-ethylmaleimide-sensitive factor attachment protein receptor.

studies in *Drosophila* indicate that PCP proteins localize to the cell junctions just apical to the adherence junction (15). Interestingly, PCP proteins are initially uniformly distributed around subapical plasma membranes and their asymmetrical localizations precede all other signs of PCP during wing development in *Drosophila* (16). Corresponding to this, the alignment of noncentrosomal microtubules are reorganized so that the majority of noncentrosomal microtubules are aligned along the proximal–distal axis with an excess of the plus ends oriented distally prior to the onset of the PCP signaling events (13, 14, 17). This microtubule dynamics are controlled by Dachsous and Fat implicating that the Dachsous/Fat/Four-jointed pathway may provide long-range directional information to reorganize the microtubule cytoskeleton for polarized delivery of PCP proteins (17).

Newly synthesized integral PCP proteins are delivered along the secretory transport pathway to the plasma membrane where they perform their physiological functions. Packaging of Vangl2 into vesicles at the ER, the first step of the secretory transport pathway, depends on one of the COPII subunits, Sec24B (18). The selectivity of this sorting is illustrated by the behavior of the Vangl2 cytosolic, C-terminal looptail mutant protein, which is unable to be packaged into COPII vesicles and thus cannot be exported out of the ER (18). Correspondingly, the looptail mutation of *Vangl2* or a mutation in *Sec24B* causes severe defects in neural tube closure during mouse embryonic development (18).

The *trans*-Golgi network (TGN) is another important station in the secretory transport pathway. At the TGN, elaborate cargo sorting machineries are employed to accurately package the correct cargo molecules into the corresponding transport carriers that are targeted to specific destinations (19). Defects in protein sorting at the TGN cause mistargeting of a variety of cargo molecules and induce various physiological defects (19). Understanding how PCP proteins are sorted into transport vesicles at the TGN will not only provide important information to explore how they are delivered to the plasma membrane but also reveal novel insights into how their asymmetric localizations are established.

Several key participants in TGN sorting have been identified, and these include small GTPases of the Arf family and cargo adaptors. Upon GTP binding, the Arf proteins undergo conformational changes in which the N-terminal lipid-binding motif is exposed to bind TGN membranes and the switch domains change the orientation to recruit various cytosolic cargo adaptors (20, 21). Once recruited on the TGN membranes, cargo adaptors bind cargo molecules thereby enriching them into transport vesicles (19). Sorting of a subset of soluble cargo proteins at the TGN is regulated by the actin-severing proteins ADF/cofilin, the lumenal Golgi-resident protein (Cab45), and the secretory pathway Ca^{2+}-ATPase isoform 1 (SPCA1) (22–25).

We have used mammalian cells as a model system to investigate the molecular mechanisms of PCP sorting. This system allowed us to perform not only microscopy and biochemical assays, but also the *in vitro* assay combined with biochemical manipulations, and thus to define the sorting signals and binding sites. Our previous analysis indicates that sorting of Vangl2 at the TGN depends on one of the Arf family proteins, Arfrp1, and the clathrin-associated adaptor protein complex-1 (AP-1) (26). Further analysis indicates that Arfrp1–AP-1 interaction opens the cargo-binding pocket of AP-1 to allow AP-1 to directly interact with the tyrosine sorting motif on the Vangl2 cytosolic domain (26). Interestingly, unlike Vangl2, TGN export of Fzd6 is independent of Arfrp1 and AP-1 suggesting that TGN export of Vangl2 and Fzd6 are mediated by different cargo sorting machineries (26). In this study, we sought to utilize mammalian cells to analyze whether Vangl2 and Fzd6 are packaged into different vesicles at the TGN and to investigate the molecular mechanism that mediates TGN export of Fzd6.

Results

Vangl2 and Fzd6 are packaged into separate vesicles in an assay that reconstitutes vesicle budding from the TGN in vitro

We previously demonstrated that TGN export of Vangl2 and Fzd6 depends on distinct cargo sorting machineries. One possible consequence of this behavior is that Vangl2 and Fzd6 may be sorted into separate vesicles. To test this, we reconstituted release of Vangl2 and Fzd6 into vesicles from the TGN *in vitro* and then tested whether the two proteins were packaged together or separately. A TGN vesicle-budding reaction using digitonin-permeablized cells has been reported (27). We performed the TGN vesicle-budding assay using COS7 cells transfected with HA-Fzd6 or HA-Vangl2 (Fig. 1*A*). After a 20 °C incubation, HA-Fzd6 showed a strong TGN-accumulated pattern with no detectable surface-localized pattern in over 80% of the expressing cells (Fig. S1, *A–C*, and quantification in *G*). When cells were shifted to 32 °C, the percentage of cells showing TGN-accumulated Fzd6 dropped to below 5% and the majority of cells showed a clear surface-localized pattern of Fzd6 (Fig. S1, *D-F*, and quantification in *G*). To reconstitute packaging of Fzd6 into vesicles at the TGN, COS7 cells were incubated at 20 °C to accumulate newly synthesized HA-Fzd6 at the TGN, then permeablized by digitonin, and incubated at 30 °C with rat liver cytosol, GTP, and an ATP regeneration system in the presence of a GTPase-defective form for Sar1A, Sar1A(H79G), to inhibit vesicle budding from the ER. After incubation, the released vesicles were separated from the donor membranes by centrifugation and analyzed by immunoblotting with antibodies against TGN46, Sec22, and the HA tag. TGN46 is an integral membrane protein that is transported from the TGN to the cell surface (28) and Sec22 is a soluble *N*-ethylmaleimide-sensitive factor attachment protein receptor (SNARE) that directly binds COPII and regulates ER-to-Golgi trafficking (29). Thus TGN46 and Sec22 can be used to monitor TGN export and ER export respectively.

Using this assay, we reproducibly detected release of TGN46, Sec22, and HA-Fzd6 into vesicles when permeabilized cells were incubated in the absence of Sar1A(H79G) (Fig. 1*B*, *lane 5*). Addition of Sar1A(H79G) to the reaction inhibited the vesicular release of Sec22 but not TGN46 and HA-Fzd6, which were packaged dependent on the concentration of cytosol (Fig. 1, *B*, *lanes 2–4*, and *C*). Export of Fzd6 depended on GTP and ATP (Fig. 1, *D*, *lane 1*, and *E*). A nonhydrolyzable analog of GTP, GMPPNP, significantly reduced packaging of Fzd6 into vesicles

(Fig. 1, *D*, *lane 4*, and *E*). HA-Fzd6 (WT) in the vesicle fraction in the presence of Sar1A(H79G) was resistant to endoglycosidase H (endo H) digestion (Fig. 1*F*, *lanes 1* and 2) but sensitive to peptide:*N*-glycosidase F (PNG-F) digestion (Fig. 1*F*, *lanes 3* and *4*, *asterisk*), whereas TGN46, which is highly *O*-glycosylated, was resistant to both endo H digestion and PNG-F diges-

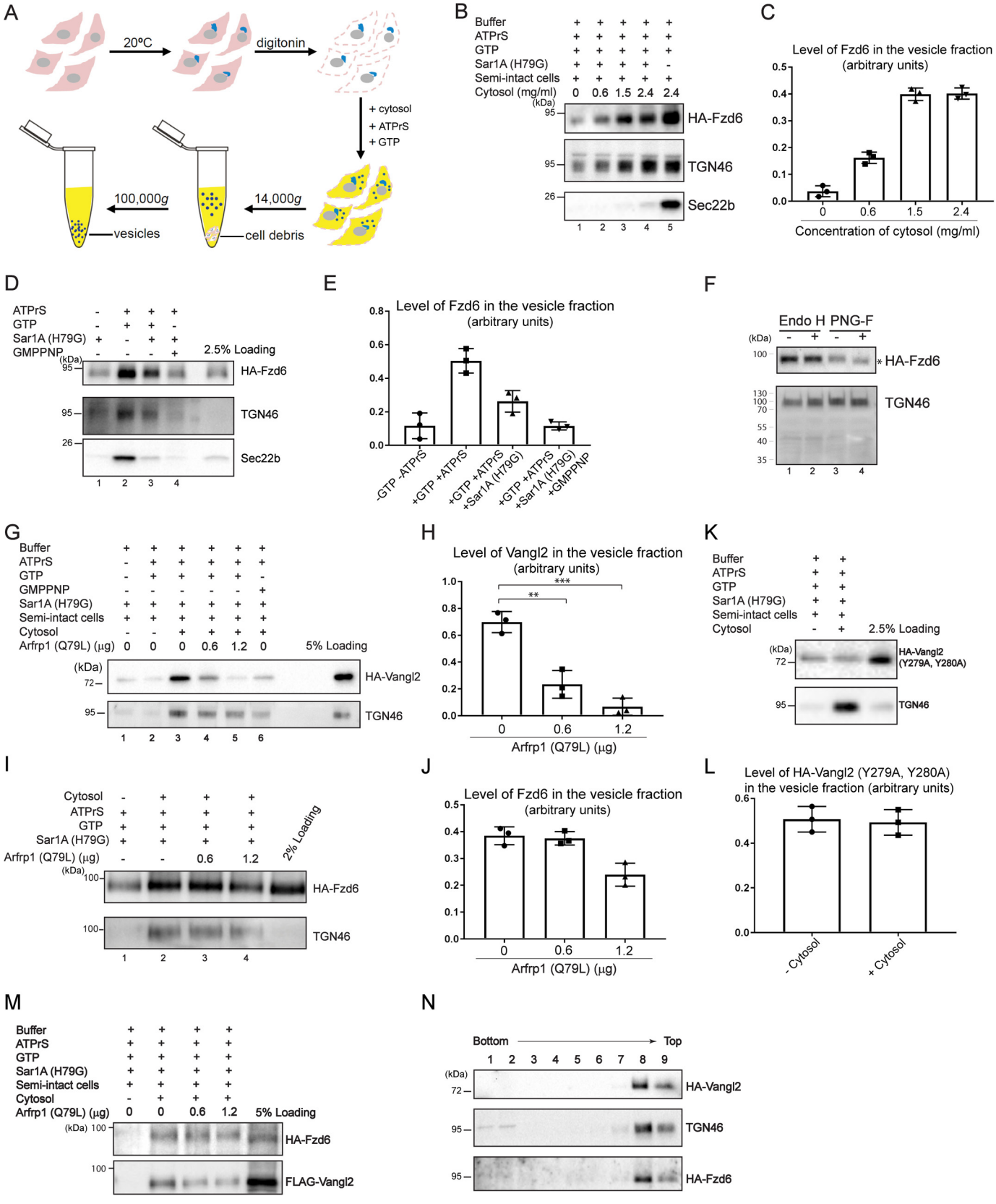

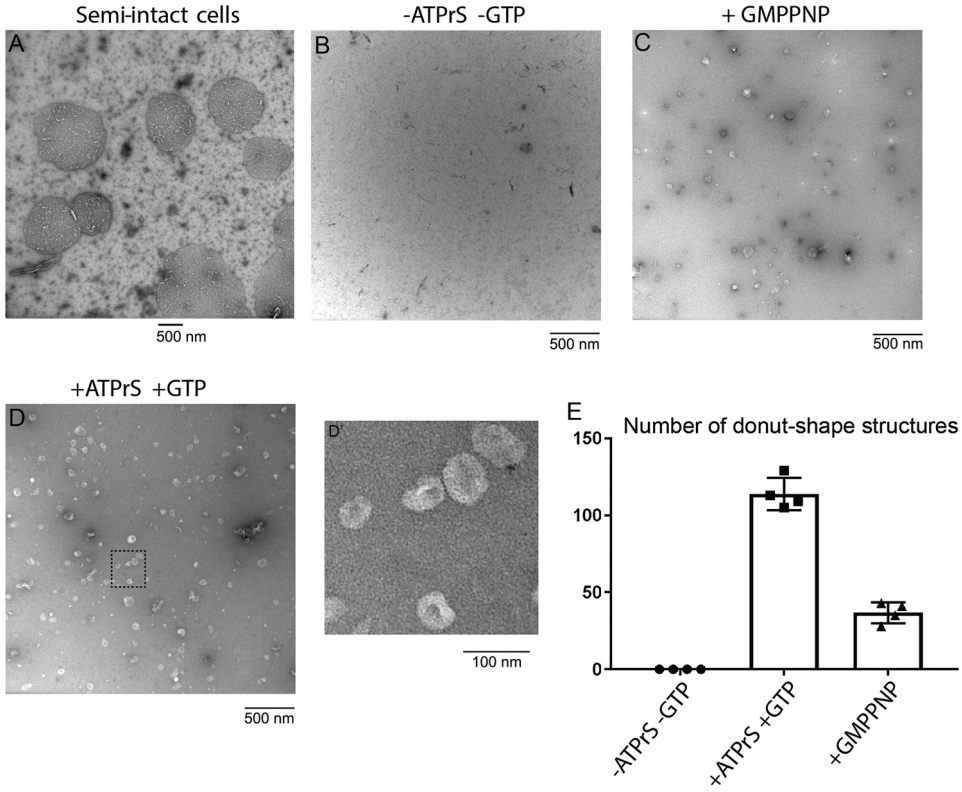

Figure 2. The buoyant membrane structures formed in the budding reaction. *A,* COS7 cells were treated with digitonin. After digitonin treatment, the permeabilized cells were analyzed by negative stain EM. *B–D,* the TGN vesicle-formation assay was performed using the indicated reagents. The buoyant membranes in the high-speed pellet fraction were isolated by density gradient flotation and analyzed by negative stain EM. *Scale bar*, 500 nm. *D′*, a magnified view of the indicated area in *D*. *Scale bar*, 100 nm. *E,* quantification of the number of the donut-shape structures (mean ± S.D., based on four fields).

tion (Fig. 1*F*), suggesting that HA-Fzd6 in the vesicle fraction contains glycans consistent with modifications in the Golgi. Based on these data, we propose that the discharge of WT Fzd6 in vesicles originates primarily at the TGN.

Using the same assay, we detected cytosol-dependent release of WT HA-Vangl2 (Fig. 1*G*) but not the tyrosine mutant (HA-Vangl2^{Y279A,Y280A}) into the vesicle fraction (Fig. 1, *K–L*). Export of Vangl2 and TGN46 into vesicles was significantly reduced by GMPPNP (Fig. 1*G*, *lane 6*). The GTPase-defective form for Arfrp1, Arfrp1(Q79L), inhibited Vangl2 release into vesicles in a concentration-dependent manner (Fig. 1, *G*, *lanes 4* and *5*, and *H*), whereas packaging of TGN46 into vesicles was only slightly inhibited by Arfrp1(Q79L) (Fig. 1*G*) indicating that the sorting of Vangl2 in vesicles originates primarily at the TGN. We then analyzed the effects of the Arfrp1(Q79L) mutant on Fzd6 release into vesicles. The result indicates that, at the lower concentration, Arfrp1(Q79L) did not affect Fzd6 release into vesicles (Fig. 1, *I*, *lane 3*, and *J*). At the higher concentration, Arfrp1(Q79L) partially inhibited release of Fzd6 in the vesicle fraction (Fig. 1, *I*, *lane 4*, and *J*). This analysis suggests that Arfrp1(Q79L) has a stronger inhibiting effect on vesicular release of Vangl2 than Fzd6. We then analyzed the effects of Arfrp1(Q79L) on release of Fzd6 and Vangl2 into vesicles in cells co-expressing these two cargo proteins. The result indicates that the Arfrp1(Q79L) mutant inhibited Vangl2 release into vesicles (Fig. 1*M*). In contrast, Arfrp1(Q79L) had a weaker inhibiting effect on Fzd6 release into vesicles than Vangl2 release into vesicles (Fig. 1*M*).

Vangl2, Fzd6, and TGN46 were all packaged into buoyant membranes (Fig. 1*N*). We used negative stain EM to visualize the morphology of the buoyant membrane structures produced in the *in vitro* budding reaction. The digitonin-treated COS7 cells were visualized by negative stain EM (Fig. 2*A*). We detected numerous donut-shaped structures in the buoyant membrane fraction (Fig. 2, *D–D′*, and *E*). The average diameter and standard deviation of all of the structures seen on the grids

Figure 1. The *in vitro* assay that reconstitutes packaging of Fzd6 and Vangl2 into vesicles from the TGN. *A,* diagram showing the *in vitro* assay that reconstitutes vesicle release from the TGN. *B–F,* COS7 cells were transfected with WT HA-Fzd6. On day 1 after transfection, the TGN vesicle-budding reaction was performed using the indicated reagents (*B–E*). The levels of Fzd6 in the vesicle fraction from the vesicle-formation assay performed using different concentrations of cytosol (*C*) or using the indicated reagents (*E*) were quantified ($n = 3$, mean ± S.D.). Vesicle fraction was untreated or incubated with endo H or PNG-F and then analyzed by immunoblot (*F*). *G–M,* COS7 cells were transfected with HA-Vangl2 WT (*G* and *H*) or HA-Fzd6 WT (*I* and *J*) or the Vangl2 mutant bearing mutations in the tyrosine sorting motif (*K* and *L*) or co-transfected with HA-Fzd6 and FLAG-Vangl2 (*M*). On day 1 after transfection, TGN vesicle release reaction was performed using the indicated reagents and vesicle fractions were analyzed by immunoblot. The levels of Fzd6 or Vangl2 in the vesicle fraction from the vesicle-formation assay performed using different concentrations of Arfrp1(Q79L) (*H* and *J*) or performed in the presence or absence of cytosol (*L*) were quantified ($n = 3$, mean ± S.D.). *N,* TGN vesicle release reaction was performed in COS7 cells transfected with HA-Vangl2 or HA-Fzd6. The vesicle fractions were evaluated by density gradient flotation. Quantification analysis was performed based on three independent replicates. In each replicate of the experiment, the intensity of the protein of interest in each reaction condition was normalized to the sum of the intensities of that protein from all reaction conditions performed in that replicate. *Triple* and *double asterisks* in *H* indicate $p < 0.01$ and $p < 0.001$ respectively. *ATPrS*, ATP regeneration system.

is 47.15 ± 22.29 nm. The donut shape probably represented vesicles collapsed by the negative stain procedure. When we performed the vesicle-budding reaction in the absence of GTP and an ATP regeneration system or in the presence of the non-hydrolysable GTP analog, GMPPNP, the number of donut-shaped structures was significantly reduced (Fig. 2, *B* and *E*, *C* and *E*). These analyses indicate that the nonsedimenting membranes in the budding reaction are transport vesicles not fragments of the Golgi or reformed ministacks.

To test whether Vangl2 and Fzd6 were packaged into vesicles together or separately, we performed the TGN vesicle-budding assay using COS7 cells co-transfected with FLAG-Vangl2 and HA-Fzd6 in which ~80% of the transfected cells co-expressed both constructs. We then immunoisolated the vesicles containing FLAG-Vangl2 using an antibody against the FLAG tag. The immunoisolation approach robustly captured Vangl2-enriched vesicles (Fig. 3, *A* and *B*). Strikingly, the immunoisolated Vangl2-enriched vesicles did not contain Fzd6 or TGN46 (Fig. 3, *A* and *C*). Likewise, TGN46 was not detected in vesicles isolated using a Fzd6 construct containing a FLAG tag in the C-terminal cytosolic domain (Fig. 3, *D–F*). As a control for our vesicle isolation experiment, we performed the vesicle-formation assay using cells co-transfected with FLAG-Vangl2 and HA-Vangl2 and then immunoisolated the vesicles containing FLAG-Vangl2. We found a fraction of the vesicles enriched with HA-Vangl2 was co-isolated with FLAG-Vangl2 (Fig. 3, *G–I*), suggesting that the separation of Vangl2 and Fzd6 was not due to disruption of vesicles. The fraction of vesicles enriched with HA-Vangl2 that were not co-isolated with FLAG-Vangl2 may be derived from cells expressing HA-Vangl2 but not FLAG-Vangl2. We analyzed the morphology of the immunoisolated vesicles by negative stain EM. The structures in the immunoisolated vesicle fraction containing Fzd6-FLAG or FLAG-Vangl2 showed donut shapes (Fig. 3, *J–K*), which are similar to the morphology we observed in the buoyant membrane fraction from the vesicle-formation assay (Fig. 2*D*). We did not detect these donut-shaped structures in the control experimental group in which the budding assay was performed without cytosol. There were no clear vesicle coat structures surrounding the immunoisolated vesicles possibly due to the reason that vesicle coat proteins were released from the vesicles after a 2-day period to immunoisolate the vesicles. Another possibility is that the immunoisolation works only for uncoated vesicles as the coat may block the antibody–antigen interaction. These results indicate that Vangl2, Fzd6, and TGN46 are packaged into separate vesicles.

Clathrin and epsinR regulate sorting of Fzd6 at the TGN

An HA-Fzd6 mutant construct lacking the C-terminal cytosolic domain (HA-Fzd6-Δcyto) accumulated at the juxtanuclear area and colocalized with a TGN marker (Golgin97) (Fig. 4, *A–F*), suggesting that this domain of Fzd6 is important for export of Fzd6 from the TGN. HA-Fzd6-Δcyto mutant was incorporated into vesicles in a budding reaction conducted in the absence of Sar1A(H79G) (Fig. 4*G*, *lane 2*). However, in the presence of Sar1A(H79G), packaging of the HA-Fzd6-Δcyto mutant into vesicles was nearly completely blocked (Fig. 4, *G*, *lane 3*, and *H*), suggesting that HA-Fzd6-Δcyto folded well enough to be packaged into COPII vesicles at the ER but lacked information or a structure necessary for sorting into vesicles packaged at the Golgi membrane. Moreover, the N-terminal one-third region of the Fzd6 cytosolic domain was sufficient to restore Sar1A(H79G)-insensitive packaging of Fzd6 into vesicles (Fig. 4, *I*, *lane 3*, and *J*).

To identify the molecular machinery that regulates sorting of Fzd6 at the TGN, we analyzed whether clathrin is an important regulator that interacts with Fzd6. We detected a weak interaction between clathrin heavy chain (CHC) and Fzd6 through an immunoprecipitation experiment (Fig. S2*A*). The weak interaction was possibly due to the reason that clathrin interacts with Fzd6 indirectly through clathrin adaptors. As a second approach to test the interaction between Fzd6 and clathrin, we performed GST-pulldown experiments by incubating purified GST-tagged Fzd6 cytosolic domain fragments with cytosol prepared from COS7 cells. We found that clathrin from cell lysates was pulled down by the full-length Fzd6 C-terminal cytosolic domain (aa 497–709), Fzd6 C-terminal cytosolic domain depleted of the conserved KT*XXX*W motif that binds the PDZ domain of Dishevelled (aa 504–709) and the first one-third region of the Fzd6 C-terminal cytosolic domain (aa 497–567) (Fig. S2*B*, *lanes 1–3*). In contrast, the last two-thirds region of the Fzd6 C-terminal cytosolic domain (aa 568–709) did not pulldown clathrin (Fig. S2*B*, *lane 4*). We then performed siRNA knockdown analysis to test whether CHC mediates TGN export of Fzd6. We used HeLa cells for our knockdown analysis because most of the commercially available pre-designed siRNAs are against human proteins. The expression of CHC was significantly reduced after siRNA treatment (Fig. 5*G*). Around 85% of siRNA-treated cells showed strong accumulations of HA-Fzd6 at the juxtanuclear area, colocalized with the TGN marker, Golgin97, whereas only 13% of mock-treated cells showed TGN-accumulated Fzd6 (Fig. 5, *A–F* and *H*). This suggests that CHC is important for TGN export of Fzd6. Knockdown of CHC also caused accumulations of Vangl2 at the TGN indicating that both Vangl2 and Fzd6 depend on CHC for traffic from the TGN (Fig. 5*H*). In contrast, knockdown of CHC did not affect TGN export of an apical cargo, p75-GFP (Fig. 5*H*) (30).

Clathrin interacts with cargo molecules through the clathrin-adaptor proteins. We analyzed the localizations of Fzd6 in HeLa cells treated with siRNAs against some of the TGN- and endosome-localized clathrin adaptor or adaptor subunits including the γ subunit of AP-1 (γ1), the δ subunit of AP-3 (δ3), or epsinR. Cells treated with each of these siRNAs did not show detectable defects in HA-Fzd6 localization at steady state, possibly due to the presence of functional redundancy among the clathrin adaptors. To test whether knockdown of a specific clathrin adaptor can cause a kinetic delay of TGN export of Fzd6, we incubated HeLa cells at 20 °C in the presence of cycloheximide to synchronize a pool of newly-synthesized HA-Fzd6 in the TGN. As the HA tag is localized on the extracellular domain of Fzd6, we performed a surface-labeling experiment to label the surface-localized HA-Fzd6. After a 20 °C incubation, HA-Fzd6 was accumulated at the juxtanuclear area, colocalized with TGN46 and the majority of cells showed no detectable surface-localized Fzd6 (Fig. 6, *A–H*). When cells were shifted to 32 °C, Fzd6 in most control siRNA-treated cells showed a

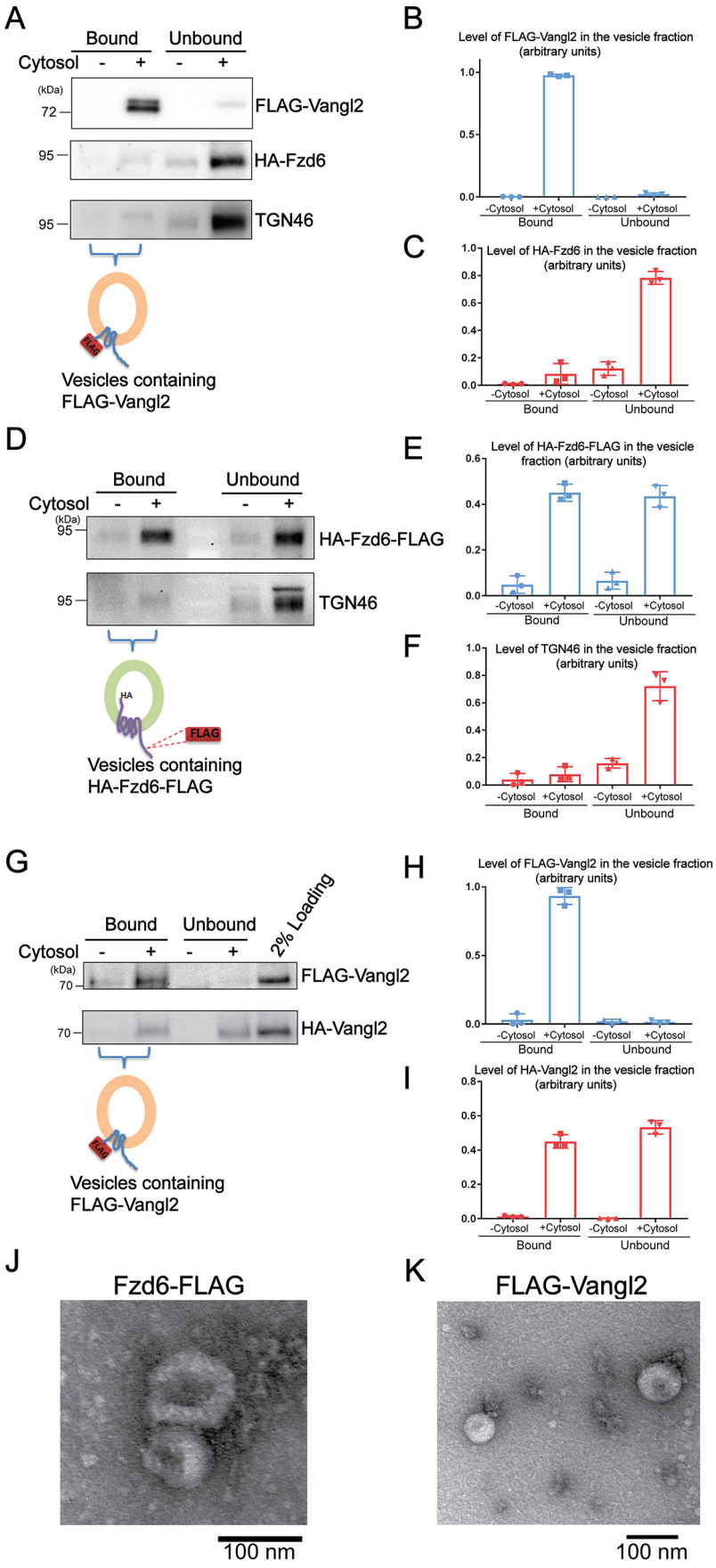
A
Bound
Unbound
Cytosol - + - +
(kDa)
72
FLAG-Vangl2
95
HA-Fzd6
95
TGN46
FLAG
Vesicles containing
FLAG-Vangl2
B
Level of FLAG-Vangl2 in the vesicle fraction
(arbitrary units)
1.0
0.5
0.0
-Cytosol +Cytosol -Cytosol +Cytosol
Bound
Unbound
C
Level of HA-Fzd6 in the vesicle fraction
(arbitrary units)
1.0
0.8
0.6
0.4
0.2
0.0
-Cytosol +Cytosol -Cytosol +Cytosol
Bound
Unbound
D
Bound
Unbound
Cytosol - + - +
(kDa)
95
HA-Fzd6-FLAG
95
TGN46
HA
FLAG
Vesicles containing
HA-Fzd6-FLAG
E
Level of HA-Fzd6-FLAG in the vesicle
fraction (arbitrary units)
0.6
0.4
0.2
0.0
-Cytosol +Cytosol -Cytosol +Cytosol
Bound
Unbound
F
Level of TGN46 in the vesicle fraction
(arbitrary units)
1.0
0.8
0.6
0.4
0.2
0.0
-Cytosol +Cytosol -Cytosol +Cytosol
Bound
Unbound
G
Bound
Unbound
2% Loading
Cytosol - + - +
(kDa)
70
FLAG-Vangl2
70
HA-Vangl2
FLAG
Vesicles containing
FLAG-Vangl2
H
Level of FLAG-Vangl2 in the vesicle fraction
(arbitrary units)
1.0
0.5
0.0
-Cytosol +Cytosol -Cytosol +Cytosol
Bound
Unbound
I
Level of HA-Vangl2 in the vesicle fraction
(arbitrary units)
0.8
0.6
0.4
0.2
0.0
-Cytosol +Cytosol -Cytosol +Cytosol
Bound
Unbound
J
Fzd6-FLAG
100 nm
K
FLAG-Vangl2
100 nm

detectable surface-localized pattern but also a certain degree of TGN- and ER-localized pattern (Fig. 6, *I–L*). The remaining Fzd6 at the TGN and the ER area after the temperature shift condition may be caused by overexpression of Fzd6. Another possible reason is that cycloheximide may not completely inhibit the synthesis of the exogenously overexpressed Fzd6. It is also possible that some of the TGN-accumulated Fzd6 was retrieved back to the ER after temperature shift. We then quantified the percentage of cells showing a detectable surface pattern of Fzd6 at the same exposure time. After the temperature was released to 32 °C, around 70% of cells treated with control siRNA showed a detectable surface pattern (Fig. 6*V*). Through this method, we found that cells treated with siRNA against one of the TGN-localized cargo adaptor, epsinR, showed a significant reduction of the percentage of cells showing surface-localized Fzd6 (Fig. 6, *M–P*, *T,* and *V*), whereas knockdown of γ1 or δ3 did not affect surface delivery of Fzd6 (Fig. S3, *A–C*). The majority of cells treated with siRNA against γ1 showed strong accumulations of HA-Vangl2 at the juxtanuclear area at the steady state (Fig. S3, *D–I*), consistent with our previous analysis (26). In contrast, knockdown of epsinR did not cause a defect in the TGN export of HA-Vangl2 (Fig. 6*W*). These analyses indicate that TGN export of Vangl2 and Fzd6 depends on distinct cargo sorting machineries.

We tested whether the phenotype of epsinR knockdown can be rescued by expressing an siRNA-resistant epsinR construct by mutating the siRNA-targeting site, and fused this construct to a FLAG tag and an IgG-binding ZZ domain (epsinR^{RE}-FLAG). Western blot analysis indicates that expression of the mutant form but not the endogenous form of epsinR was resistant to siRNA treatment (Fig. 6*U*). Expression of epsinR^{RE}-FLAG restored the percentage of cells with detectable surface HA-Fzd6 to the control level (Fig. 6, *Q–S* and *V*), suggesting that expressing epsinR rescues the knockdown phenotype. We analyzed the localization of Fzd6 in cells that were transfected with another siRNA that targets a different region in epsinR. HeLa cells transfected with this siRNA also showed a reduction of the expression level of epsinR (Fig. S4*Q*) and a significant reduction of the percentage of cells showing surface-localized Fzd6 (Fig. S4, *I–P* and *R*).

To test whether epsinR interacts with Fzd6, we performed GST-pulldown experiments using GST-tagged Fzd6 cytosolic domain fragments (aa 497–467 and 568–709) and lysates from COS7 cells expressing epsinR fused to FLAG and an IgG-binding ZZ domain (used in combination to increase the specificity for affinity purification) at its C terminus (hereafter referred to as epsinR-FLAG). A GST fusion containing the N-terminal one-third region of the Fzd6 cytosolic domain bound epsinR-FLAG in COS7 cell lysates, whereas the GST fusion containing the other two-thirds of the Fzd6 cytosolic domain did not (Fig. 7*A*). Epsins are composed of an ENTH domain at the N terminus followed by a long, unfolded domain. The unfolded domain but not the ENTH domain of epsinR interacted with the GST-tagged Fzd6 cytosolic domain (Fig. 7*B*).

We then purified epsinR by immunoprecipitation from cell lysates of COS7 cells expressing epsinR-FLAG. FLAG-tagged epsinR co-purified with CHC (Fig. 7*C*, *lanes 1* and *2*). The immunoprecipitated epsinR-CHC complex bound the N-terminal one-third region of the Fzd6 cytosolic domain but not the other part of Fzd6 cytosolic domain (Fig. 7*D*).

The results from the GST-pulldown assay are consistent with our vesicular release assay (Fig. 4, *I* and *J*) suggesting that the N-terminal one-third region of the Fzd6 cytosolic domain contains a sorting motif that is important to bind the epsinR-CHC complex for incorporation of Fzd6 into vesicles. Sequence alignment of this region in Fzd6 and another PCP protein, Frizzled3, across species revealed several conserved motifs including a KT*XXX*W motif (Fig. 8*A*, *green box*) and a polybasic motif (Fig. 8*A*, *red box*). We found that deleting the polybasic motif in Fzd6 resulted in the accumulation of mutant Fzd6 at the juxtanuclear area, colocalized with Golgin97 in the majority of the cells (Fig. 8, *B–G*). In contrast, deleting the KT*XXX*W motif or other conserved regions in the Fzd6 cytosolic domain had no effect on Fzd6 localization.

To test whether the polybasic motif was critical for packaging of Fzd6 into transport vesicles at the TGN, we performed the TGN vesicle budding reaction using HA-tagged Fzd6 WT or the Fzd6 polybasic mutant construct. The efficiency of packaging of mutant Fzd6 into transport vesicles was significantly reduced (Fig. 8, *H* and *I*). To test whether the polybasic motif was important to bind epsinR, we compared the efficiency of GST pulldown using wild type and mutant versions of HA-tagged Fzd6. Fzd6 lacking the polybasic region displayed reduced binding to epsinR-FLAG in COS7 cell lysates (Fig. 8, *J* and *K*) and reduced binding to the immunoprecipitated epsinR-CHC complex (Fig. 8, *L* and *M*). These analyses suggest that epsinR forms a stable complex with clathrin and this complex binds to the polybasic motif on the Fzd6 cytosolic domain to mediate sorting of Fzd6 into transport vesicles at the TGN.

Binding of Fzd6 to epsinR causes disassociation of epsinR from AP-1

EpsinR and AP-1 are both clathrin adaptors that interact with each other. To test whether binding of AP-1 to epsinR interferes with the interaction between epsinR and Fzd6, we mutated the AP-1–binding motif on epsinR. As previously reported (31), mutating the two key amino acids on epsinR, Asp-349 and Asp-371, blocked the interaction between epsinR and AP-1 (Fig. 9*A*). We then performed a GST-pulldown experiment using purified GST-tagged Fzd6 cytosolic fragment (aa

Figure 3. Fzd6, Vangl2, and TGN46 are packaged into separate vesicles. *A–I,* COS7 cells were co-transfected with HA-Fzd6 and FLAG-Vangl2 (*A–C*) or transfected with HA-Fzd6-FLAG (*D–F*) or co-transfected with HA-Vangl2 and FLAG-Vangl2 (*G–I*). Day 1 after transfection, a TGN vesicle release reaction was performed. The medium speed supernatant fractions were incubated with anti-FLAG M2 affinity gel. The bound fraction was eluted using FLAG peptides and the unbound fraction was centrifuged at high speed to sediment small vesicles. The bound and unbound fractions were analyzed by immunoblot. The levels of Fzd6, Vangl2, or TGN46 in the vesicle fraction were quantified based on three independent replicates (*B*, *C*, *E*, *F*, *H,* and *I*, mean ± S.D.). In each replicate of the experiment, the intensity of the protein of interest in each reaction condition was normalized to the sum of the intensities of that protein from all reaction conditions performed in that replicate. *J–K,* the TGN vesicle-formation assay was performed using COS7 cells expressing FLAG-Vangl2 or FLAG-Fzd6. The medium speed supernatant fractions were incubated with anti-FLAG M2 affinity gel. The bound fraction was eluted using FLAG peptides and the eluted fraction was analyzed by negative stain EM. *Scale bar*, 100 nm.

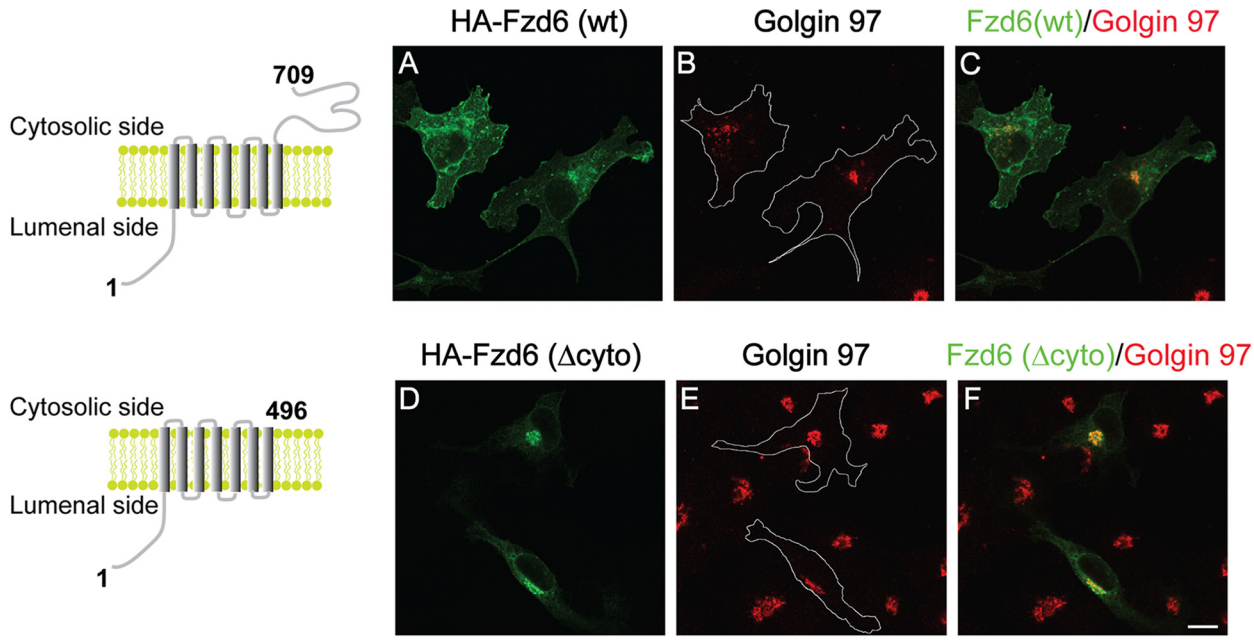
HA-Fzd6 (wt)
Golgin 97
Fzd6(wt)/Golgin 97
709
Cytosolic side
Lumenal side
1
A
B
C
HA-Fzd6 (Δcyto)
Golgin 97
Fzd6 (Δcyto)/Golgin 97
Cytosolic side
496
Lumenal side
1
D
E
F

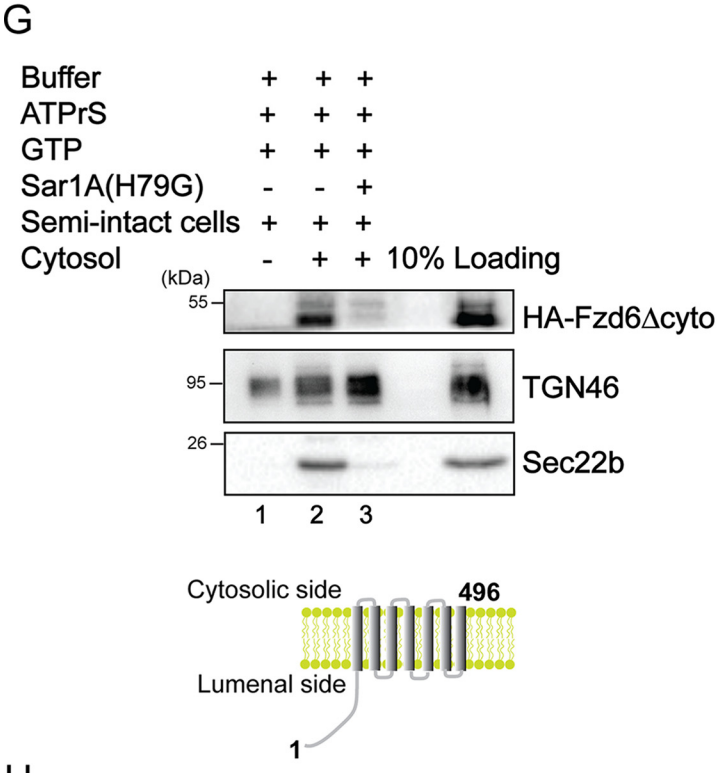
G
Buffer + + +
ATPrS + + +
GTP + + +
Sar1A(H79G) - - +
Semi-intact cells + + +
Cytosol - + +
10% Loading
(kDa)
55
95
26
HA-Fzd6Δcyto
TGN46
Sec22b
1 2 3
Cytosolic side
496
Lumenal side
1

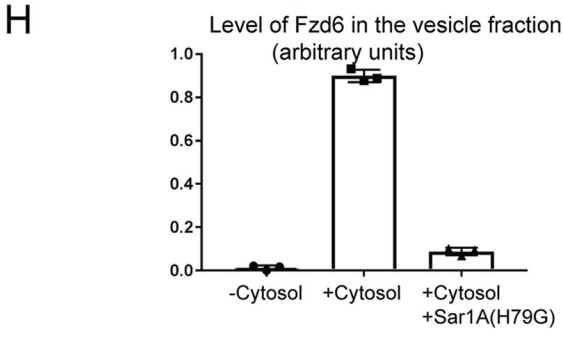
H
Level of Fzd6 in the vesicle fraction
(arbitrary units)
1.0
0.8
0.6
0.4
0.2
0.0
-Cytosol
+Cytosol
+Cytosol
+Sar1A(H79G)

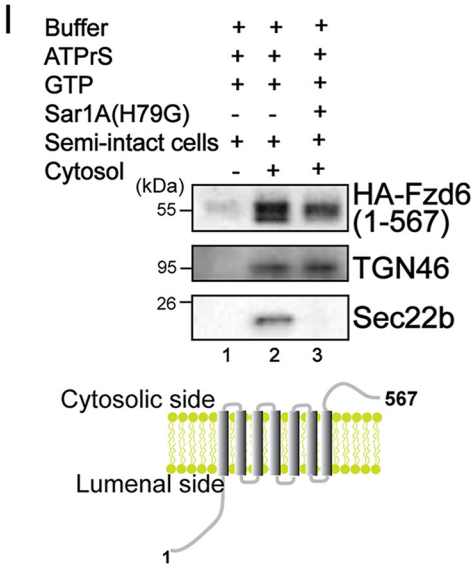
I
Buffer + + +
ATPrS + + +
GTP + + +
Sar1A(H79G) - - +
Semi-intact cells + + +
Cytosol - + +
(kDa)
55
95
26
HA-Fzd6
(1-567)
TGN46
Sec22b
1 2 3
Cytosolic side
567
Lumenal side
1

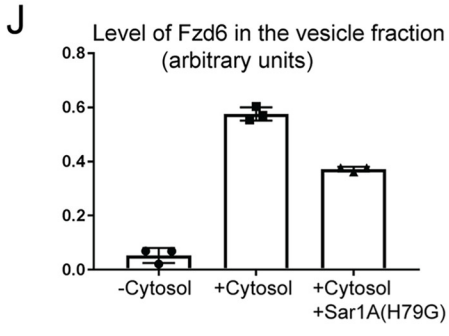
J
Level of Fzd6 in the vesicle fraction
(arbitrary units)
0.8
0.6
0.4
0.2
0.0
-Cytosol
+Cytosol
+Cytosol
+Sar1A(H79G)

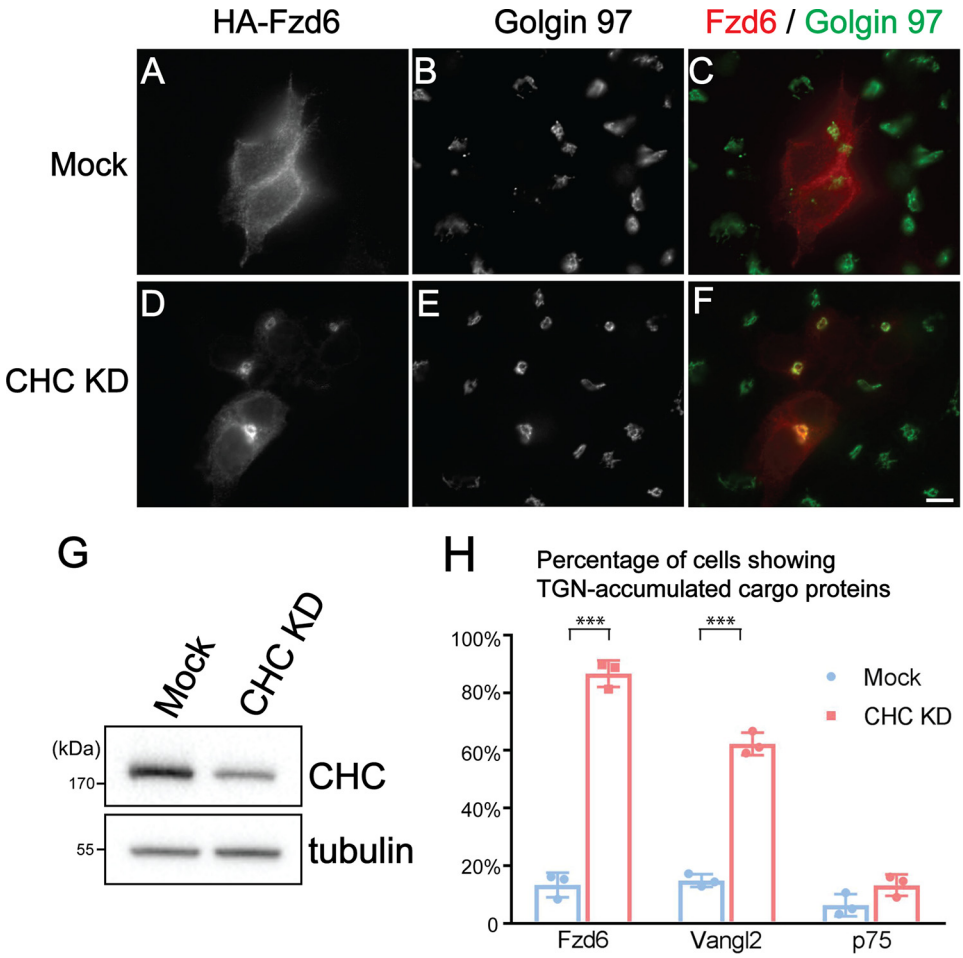

Figure 5. Clathrin heavy chain regulates TGN export of Fzd6. *A–F,* HeLa cells were mock transfected (*A–C*) or transfected with siRNA against CHC (*D–F*) and re-transfected after 48 h with plasmid encoding HA-Fzd6. After an additional 24 h, cells were analyzed by immunofluorescence. *Scale bar*, 10 μm. *G,* HeLa cells were mock transfected or transfected with siRNA against CHC. On day 3 after transfection, total cell lysates were analyzed by immunoblot. *H,* quantification of the percentage of cells showing TGN-accumulated Fzd6, Vangl2, and p75 in cells treated with control siRNA or siRNA against CHC (mean ± S.D.; $n = 3$; >150 cells counted for each experiment). *Triple asterisks* in *H* indicate $p < 0.001$.

497–567) and cell lysates from HEK293T cells transfected with plasmids encoding a WT FLAG-tagged epsinR C terminus (epsinR ΔENTH-FLAG) or transfected with plasmids encoding an AP-1–binding deficient mutant version of the FLAG-tagged epsinR C terminus (epsinR $\Delta ENTH^{D349R,D371R}$-FLAG). Interestingly, mutating the AP-1–binding sites on epsinR enhanced the interaction between epsinR and Fzd6 (Fig. 9*B*), suggesting that binding of AP-1 to epsinR interferes with the interaction between Fzd6 and epsinR. As both Fzd6 and AP-1 bind to the C-terminal unfolded region of epsinR, we hypothesize that binding of Fzd6 to epsinR causes dissociations of AP-1 from epsinR. To test this, we immunoprecipiated the FLAG-tagged epsinR C terminus and incubated the immunoprecipiated proteins (epsinR ΔENTH IP) with purified GST-Fzd6 cytosolic domain fragments (aa 497–567 or 568–709). As expected, γ1-adaptin co-immunoprecipitated with epsinR ΔENTH-FLAG (Fig. 9*C*). The GST-Fzd6 cytosolic domain fragment (aa 497–567) but not the GST-Fzd6 cytosolic domain fragment (aa 568–709) bound to epsinR ΔENTH IP (Fig. 9*C*, *lanes 2* and *3*). Remarkably, we found that the affinity between epsinR and γ1-adaptin was significantly reduced in the presence of purified a GST-Fzd6 cytosolic domain fragment (aa 497–567) (Fig. 9*C*, *lane 2*). In contrast, a purified GST-Fzd6 cytosolic fragment (aa 568–709) did not interfere with the interaction between epsinR and γ1-adaptin (Fig. 9*C*, *lane 3*). We then performed the experiment using three different concentrations of Fzd6 (497–567), we found that coimmunoprecipitation of AP-1 was progressively reduced by increasing concentrations of Fzd6 (497–567) (Fig. 9, *D, lanes 1-3*, and *E*). In contrast, the Fzd6 cytosolic fragment depleted of the KR motif did not cause a release of AP-1 from epsinR (Fig. 9, *D, lane 4*, and *E*). These results indicate that binding of Fzd6 to epsinR causes dissociation of epsinR from AP-1 and this may allow these two cargo adaptors

Figure 4. TGN export of Fzd6 depends on the C-terminal cytosolic domain. *A–F,* COS7 cells were transfected with plasmids encoding HA-Fzd6 WT (*A–C*) or the C-terminal cytosolic domain-depletion construct (*D–F*, HA-Fzd6-Δcyto). At day 1 after transfection, the cells were analyzed by immunofluorescence. The peripheries of the cells expressing Fzd6 were highlighted in *B* and *E*. *Scale bar*, 10 μm. *G–J,* TGN vesicle release reaction was performed using COS7 cells expressing HA-Fzd6-Δcyto (*G* and *H*) or HA-Fzd6 deleted of the last two-thirds region of the C-terminal cytosolic domain (*I* and *J*, HA-Fzd6 1–567). Vesicle fractions were analyzed by immunoblot. The levels of Fzd6 in the vesicle fraction were quantified based on three independent replicates (*H* and *J*, mean ± S.D.). In each replicate of experiment, the intensity of Fzd6 in each reaction condition was normalized to the sum of the intensities of Fzd6 from all reaction conditions performed in that replicate.

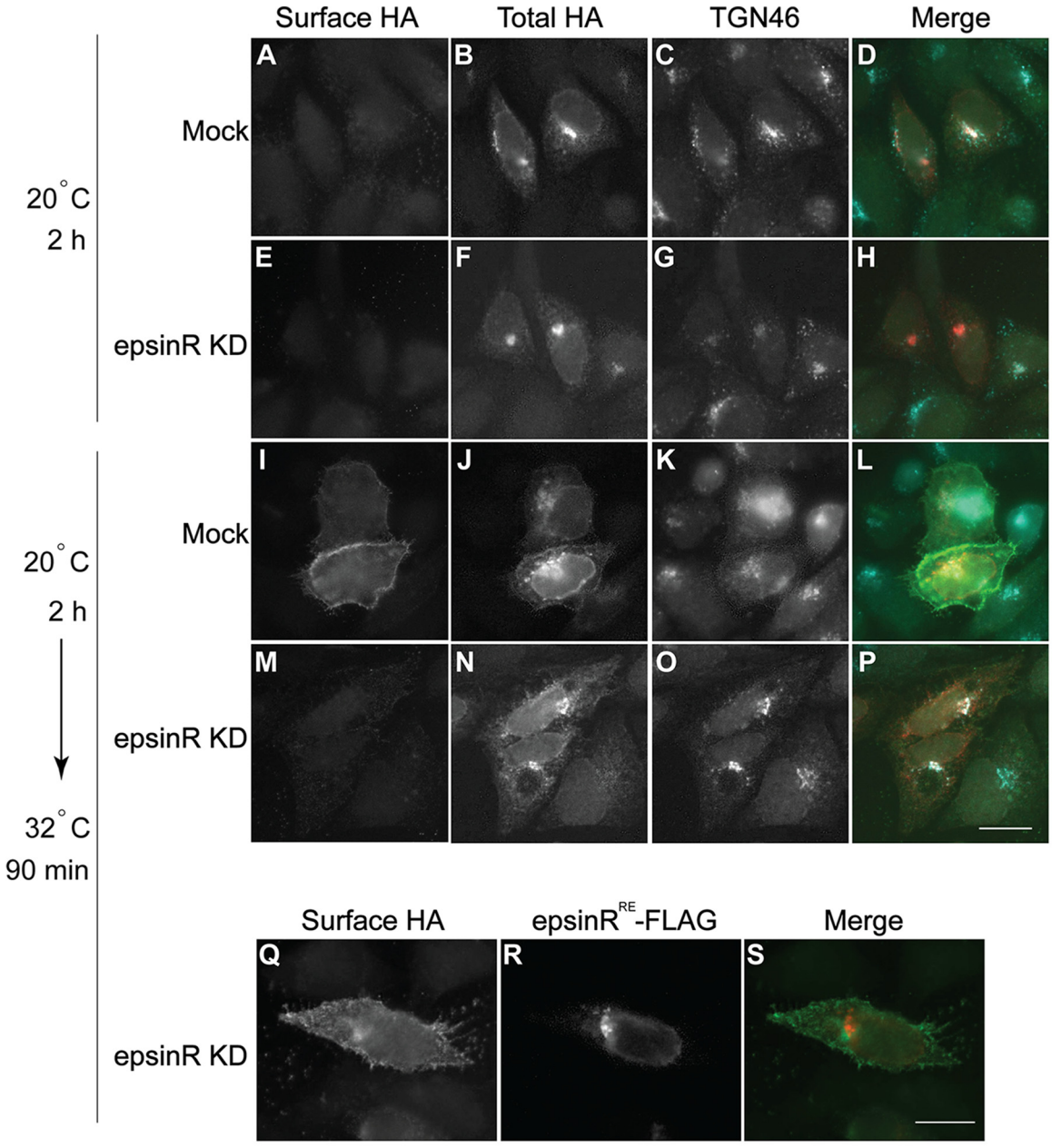
Surface HA
Total HA
TGN46
Merge
A
B
C
D
Mock
20°C
2 h
E
F
G
H
epsinR KD
I
J
K
L
Mock
20°C
2 h
M
N
O
P
epsinR KD
32°C
90 min
Surface HA
epsinR^RE-FLAG
Merge
Q
R
S
epsinR KD

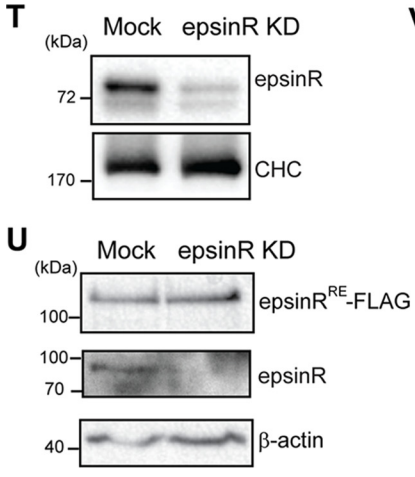
T
Mock
epsinR KD
(kDa)
72
epsinR
170
CHC
U
Mock
epsinR KD
(kDa)
100
epsinR^RE-FLAG
100
70
epsinR
40
β-actin

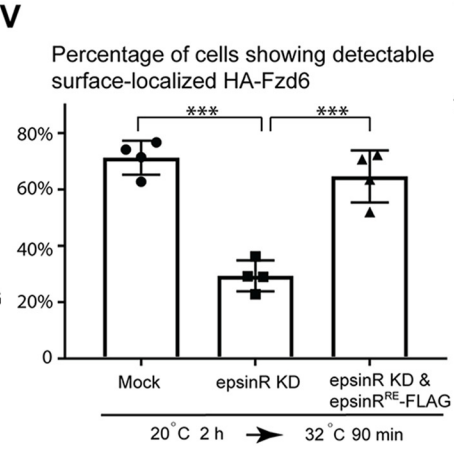
V
Percentage of cells showing detectable surface-localized HA-Fzd6
***
***
80%
60%
40%
20%
0
Mock
epsinR KD
epsinR KD & epsinR^RE-FLAG
20°C 2 h
32°C 90 min

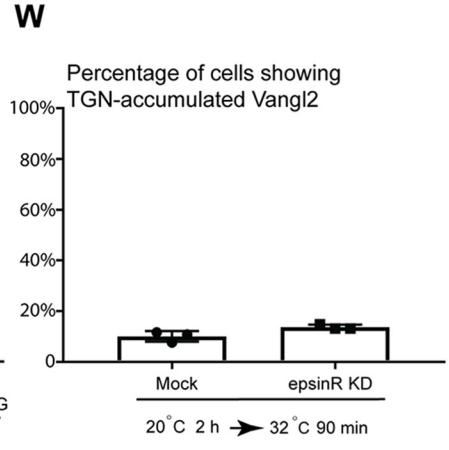
W
Percentage of cells showing TGN-accumulated Vangl2
100%
80%
60%
40%
20%
0
Mock
epsinR KD
20°C 2 h
32°C 90 min

to be separated from each other to perform distinct cargo sorting functions.

Discussion

The TGN is an essential transport hub in the secretory transport pathway. Although significant progress has been achieved in understanding biosynthetic cargo protein sorting at the TGN, several important aspects remain to be further investigated. How specific and robust is the cargo sorting process that takes place at the TGN? Are the biochemical approaches that proved crucial to understanding other coat protein-mediated vesicle budding events applicable to study sorting at the TGN? Moreover, the molecular mechanisms that regulate TGN sorting of signaling receptors that mediate important physiological and pathological processes remain to be defined.

Using a cell-free reconstitution approach that captures packaging of cargo proteins into vesicles from the TGN, we showed that the three cargo proteins, Vangl2, Fzd6, and TGN46, are packaged into separate vesicles. These analyses support a view of differential sorting of Vangl2 and Fzd6 at the TGN and suggest that the packaging of cargo proteins into transport vesicles at the TGN is highly specific with perhaps only a minor contribution by nonspecific packaging such as bulk flow. We probed the molecular mechanism that regulates packaging of Fzd6 into transport vesicles and found that epsinR forms a stable complex with clathrin that interacts with a polybasic motif on the Fzd6-cytosolic domain to facilitate its sorting into transport vesicles.

The cargo sorting process is a critical step to ensure the fidelity of protein transport along the complicated TGN exit routes. Defects in TGN sorting will cause mistargeting of proteins thereby inducing physiological defects (19). Consistent with our finding, knockdown of AP-1 subunits in the *Drosophila* wing disrupts the polarized pattern of PCP proteins and induces defects in PCP signaling processes such as multiple cellular hair defects (32). The *Drosophila* homolog of epsinR, *lqfR*, is important for various developmental processes including wing hair patterning suggesting its involvement in planar cell polarity (33, 34). However, the majority of the defects in *lqfR* mutants are rescued by exon 6 of the *lqfRa* gene encoding a domain that is homologous to Tel2, a protein that regulates telomere maintenance and DNA repair (35). In zebrafish, an insertion within an intron of the gene encoding epsinR causes defects in epidermal homeostasis (36). This phenotype is similar to that observed in zebrafish mutants bearing mutations in lethal giant larvae 2 (*ldl2*), an important regulator of cell polarity (36, 37). EpsinR and Ldl2 function synergistically in regulating epidermal homeostasis (36). The ENTH domains of two epsins in yeast, Ent1 and Ent2, bind guanine nucleotide triphosphatase-activating proteins for Cdc42 and disrupting this interaction leads to cell polarity defects (38). In mammalian cells, epsinR is important for retrograde transport of Shiga toxin, TGN46, and mannose 6-phosphate receptor from the early endosomes to the TGN (39).

EpsinR contains an N-terminal ENTH domain and a C-terminal unfolded region. The epsinR ENTH domain interacts directly with various SNAREs (40–44). We mapped the Fzd6-binding site on epsinR to the C-terminal unfolded region but not the ENTH domain, suggesting that epsinR could possibly interact simultaneously with both SNAREs and Fzd6 to package them together into transport vesicles. The C-terminal unfolded region of epsinR also binds clathrin (19). Here we showed that epsinR forms a stable complex with clathrin. By analogy to other vesicle coat proteins, it seems likely that clathrin plays an indirect role through epsinR in the sorting of Fzd6 into transport vesicles.

Currently, several sorting motifs have been identified that are recognized by clathrin adaptors. These motifs include tyrosine-based motifs that are recognized by adaptor complexes, dileucine-based motifs that are recognized by adaptor complexes and GGAs, and NP*X*Y motifs that are recognized by clathrin adaptor proteins, Dab2 and ARH (45). The C-terminal unfolded region of epsins 1–3 contains ubiquitin-interacting motifs that are implicated to interact with ubiquitinated cargo proteins (46–48). A clathrin adaptor protein, Hrb, recognizes the longin domain of the SNARE Vamp7 (49). Another group of clathrin adaptors β-arrestins recognize the phosphorylated C-terminal tail and the cytosolic surface of the transmembrane bundle of the G protein-coupled receptors (50). We found that TGN export of Fzd6 depends on a conserved polybasic motif on its C-terminal cytosolic domain. The polybasic motif also regulates TGN export of the reptilian reovirus p14 protein (51, 52). This motif mediates the interaction between activated Rab11 and p14 as detected in cell lysates (53). Thus the polybasic motif may interact with multiple binding partners. Another PCP protein, Frizzled3, also contains a polybasic motif in its C-terminal cytosolic domain indicating that the epsinR-clathrin complex may also regulate sorting of Frizzled3 at the TGN.

The C-terminal unfolded region of epsinR also directly interacts with the appendage domain of AP-1 (45). Evidence suggests that these two clathrin adaptors may be functionally related. In yeast, the epsin-related proteins, Ent3 and Ent5, function redundantly with AP-1 to regulate intracellular retention of Chs3p (54). In mammalian cells, epsinR and AP-1 are shown to depend on each other for their maximum incorporation into clathrin-coated vesicles (42). Based on proteomic analysis of purified clathrin-coated vesicles (CCVs) in control cells and in cells where epsinR is depleted by sequestering in a "knocksideways" approach, the Robinson laboratory showed that: 1) epsinR is a major, near-stoichiometric component of

Figure 6. EpsinR regulates TGN export of Fzd6. *A–S,* HeLa cells were mock transfected (*A–D* and *I–L*) or transfected with siRNA against epsinR (*E–H* and *M–S*) and re-transfected after 48 h with plasmids encoding HA-Fzd6 (*A–P*) or re-transfected with plasmids encoding epsinR^{RE}-FLAG and HA-Fzd6 (*Q–S*). On day 3 after knockdown, cells were incubated at 20 °C for 2 h (*A–H*) or incubated at 20 °C for 2 h then shifted to 32 °C for 90 min (*I–S*). After incubation, cells were analyzed by immunofluorescence. The surface-localized HA-Fzd6 and the total HA-Fzd6 were stained by mouse and rabbit anti-HA antibodies, respectively. *Scale bar*, 10 μm. *T,* HeLa cells were mock transfected or transfected with siRNA against epsinR. On day 3 after transfection, cells were analyzed by immunoblot. *U,* HeLa cells were mock transfected or transfected with siRNA against epsinR and re-transfected after 48 h with plasmids encoding epsinR^{RE}-FLAG. After an additional 24 h, cells were analyzed by immunoblot. *V,* quantification of the percentage of cells showing detectable surface-localized HA-Fzd6 (mean ± S.D.; $n = 4$; >100 cells counted for each experiment). *W,* quantification of the percentage of cells showing TGN-accumulated Vangl2 in cells treated with control siRNA or siRNA against epsinR after incubation at 32 °C (mean ± S.D.; $n = 3$; >150 cells counted for each experiment). *Triple asterisks* in *V* indicate $p < 0.001$.

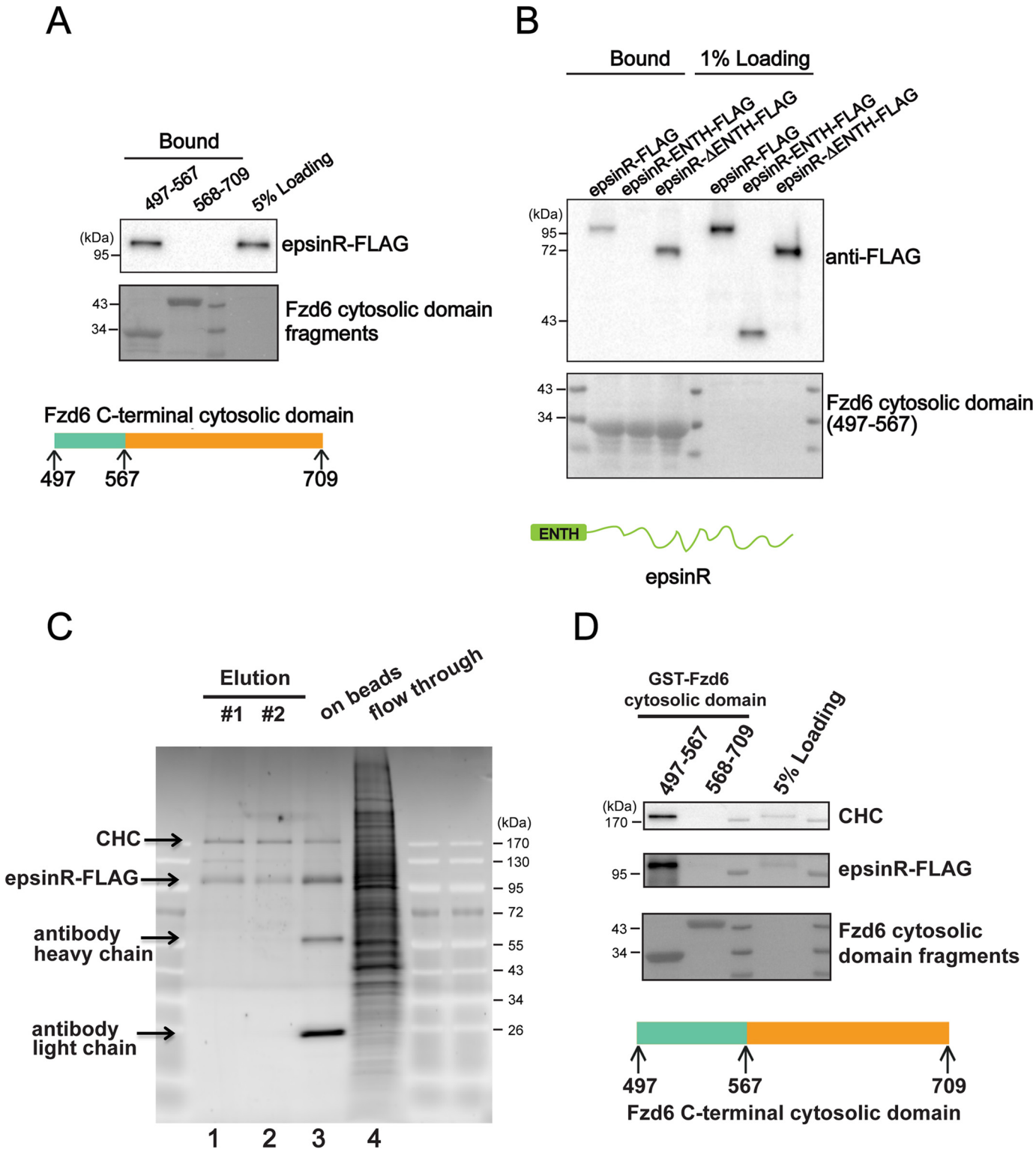

Figure 7. EpsinR forms a stable complex with clathrin that interacts with Fzd6 cytosolic domain. *A* and *B*, purified GST-tagged Fzd6 cytosolic domain fragments were incubated with lysates from COS7 cells transfected with full-length FLAG-tagged epsinR or FLAG-tagged epsinR ENTH domain or FLAG-tagged epsinR C-terminal unfolded region. After incubation, the bound fraction was analyzed by immunoblot. *C*, FLAG-tagged epsinR from cell lysates of transiently transfected COS7 cells were immunoprecipitated and the proteins were eluted using FLAG peptide (*lanes 1* and *2*), proteins remained on beads after elution (*lane 3*) and proteins in the flow-through fraction (*lane 4*) were resolved by SDS-PAGE and analyzed by silver staining. *D*, GST-tagged Fzd6 cytosolic domain fragments immobilized to GSH beads were incubated with the immunoprecipitated epsinR-CHC complex. After incubation, the bound fraction was analyzed by immunoblot.

CCVs and 2) that epsinR knocksideways blocks the production of the entire population of intracellular CCVs (55). This result would appear to conflict with our observation of a cargo-selective effect of epsinR on the traffic of Fzd6 *versus* Vangl2. The knocksideways approach, although depleting a protein more quickly than the knockdown approach, has the disadvantage of

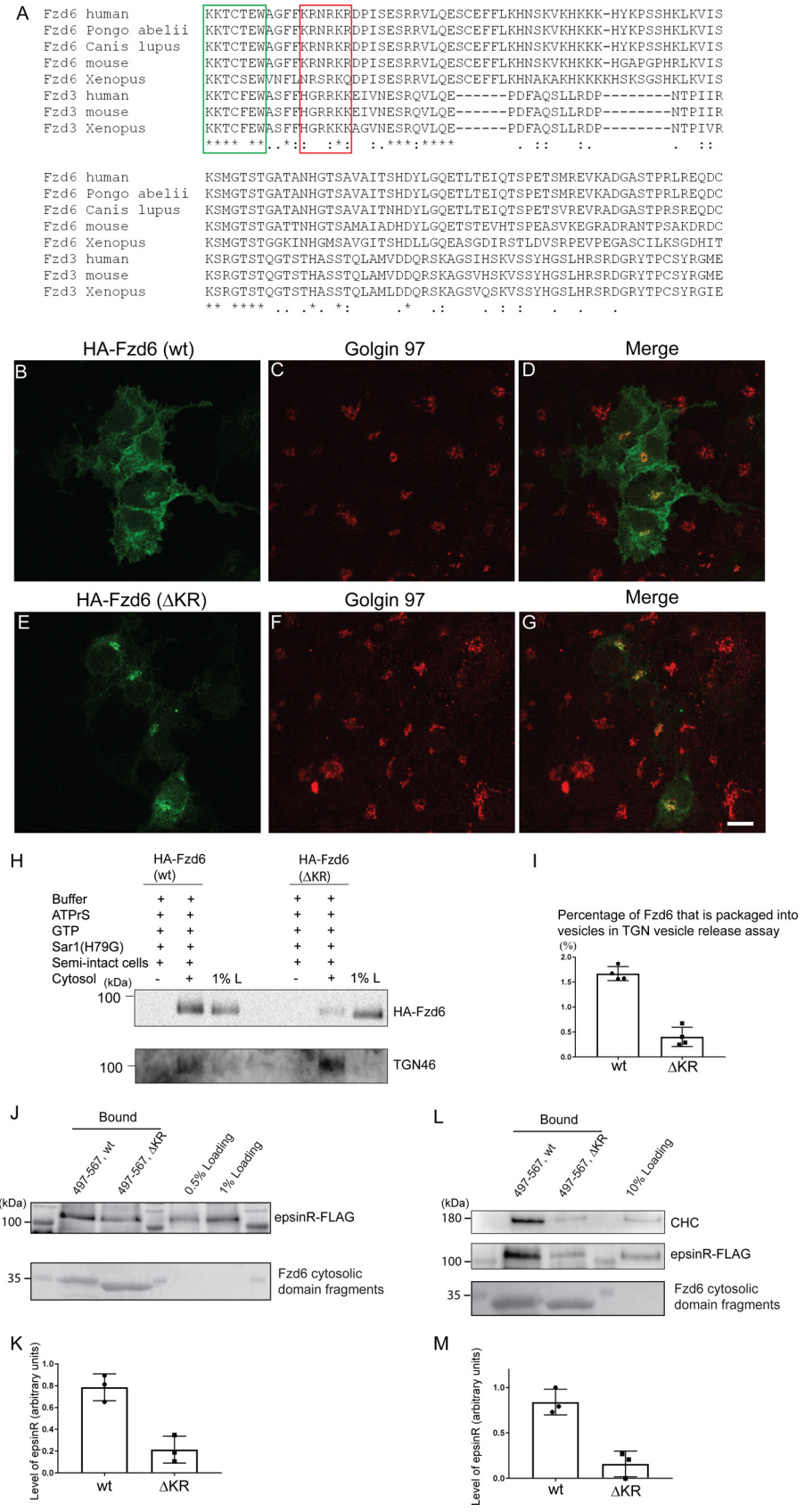
A
Fzd6 human KKTCTEWAGFFKRNRKRDPISESRRVLQESCEFFLKHNSKVKHKKK-HYKPSSHKLKVIS
Fzd6 Pongo abelii KKTCTEWAGFFKRNRKRDPISESRRVLQESCEFFLKHNSKVKHKKK-HYKPSSHKLKVIS
Fzd6 Canis lupus KKTCTEWAGFFKRNRKRDPISESRRVLQESCEFFLKHNSKVKHKKK-HYKPSSHKLKVIS
Fzd6 mouse KKTCTEWAGFFKRNRKRDPISESRRVLQESCEFFLKHNSKVKHKKK-HGAPGPHRLKVIS
Fzd6 Xenopus KKTCSEWVNFLNRSRKQDPISESRRVLQESCEFFLKHNAKAKHKKKKHSKSGSHKLKVIS
Fzd3 human KKTCFEWASFFHGRRKKEIVNESRQVLQE------PDFAQSLLRDP--------NTPIIR
Fzd3 mouse KKTCFEWASFFHGRRKKEIVNESRQVLQE------PDFAQSLLRDP--------NTPIIR
Fzd3 Xenopus KKTCFEWASFFHGRKKKAGVNESRQVLQE------PDFAQSLLRDP--------NTPIVR
Fzd6 human KSMGTSTGATANHGTSAVAITSHDYLGQETLTEIQTSPETSMREVKADGASTPRLREQDC
Fzd6 Pongo abelii KSMGTSTGATANHGTSAVAITSHDYLGQETLTEIQTSPETSMREVKADGASTPRLREQDC
Fzd6 Canis lupus KSMGTSTGATANHGTSAVAITNHDYLGQETLTEIQTSPETSVREVRADGASTPRSREQDC
Fzd6 mouse KSMGTSTGATTNHGTSAMAIADHDYLGQETSTEVHTSPEASVKEGRADRANTPSAKDRDC
Fzd6 Xenopus KSMGTSTGGKINHGMSAVGITSHDLLGQEASGDIRSTLDVSRPEVPEGASCILKSGDHIT
Fzd3 human KSRGTSTQGTSTHASSTQLAMVDDQRSKAGSIHSKVSSYHGSLHRSRDGRYTPCSYRGME
Fzd3 mouse KSRGTSTQGTSTHASSTQLAMVDDQRSKAGSVHSKVSSYHGSLHRSRDGRYTPCSYRGME
Fzd3 Xenopus KSRGTSTQGTSTHASSTQLAMLDDQRSKAGSVQSKVSSYHGSLHRSRDGRYTPCSYRGIE
HA-Fzd6 (wt)
Golgin 97
Merge
B
C
D
HA-Fzd6 (ΔKR)
Golgin 97
Merge
E
F
G
H
HA-Fzd6 (wt)
HA-Fzd6 (ΔKR)
Buffer
ATPrS
GTP
Sar1(H79G)
Semi-intact cells
Cytosol
(kDa)
1% L
1% L
100
HA-Fzd6
100
TGN46
I
Percentage of Fzd6 that is packaged into vesicles in TGN vesicle release assay
(%)
wt
ΔKR
J
Bound
497-567, wt
497-567, ΔKR
0.5% Loading
1% Loading
(kDa)
100
epsinR-FLAG
35
Fzd6 cytosolic domain fragments
L
Bound
497-567, wt
497-567, ΔKR
10% Loading
(kDa)
180
CHC
100
epsinR-FLAG
35
Fzd6 cytosolic domain fragments
K
Level of epsinR (arbitrary units)
wt
ΔKR
M
Level of epsinR (arbitrary units)
wt
ΔKR

sequestering all other proteins to which the target is tightly and quantitatively bound. Thus the knocksideways approach may cause a more general defect in the traffic of clathrin-mediated cargo, including processes that are not epsinR or AP-1-dependent. This is reflected in their previous analysis (42, 56) as mentioned under "Discussion": "However, it is important to remember that knocking down epsinR or AP-1 produces a much weaker phenotype than knocking them sideways" (55).

In the current study, we did not detect any defects in Fzd6 localization in cells depleted of AP-1 or defects in Vangl2 localization in cells depleted of epsinR. The *in vitro* vesicle-formation assay suggests that Vangl2 and Fzd6 are packaged in separate vesicles and their vesicular release depends on the AP-1-binding motif on Vangl2 and the epsinR-binding motif on Fzd6, respectively. This evidence suggests that epsinR and AP-1 can function independently of each other to regulate sorting of Vangl2 and Fzd6 at the TGN. Moreover, our results indicate that binding of Fzd6 to epsinR reduces the affinity between epsinR and AP-1. Thus the presence of a specific cargo protein, Fzd6, can cause dissociation of epsinR from AP-1 to allow them to perform distinct cargo sorting functions.

We suggest that an initial step in the establishment of epithelial cell-lateral polarity is established by the sorting of membrane-signaling proteins such as Vangl2 and Fzd6 by different Golgi vesicle-budding coats and that the final disposition of these receptors on opposing lateral surfaces of an epithelial cell are reinforced by association with PCP proteins at the proximal and distal plasma membrane domains. In the *Drosophila* wing, Frizzled and Dishevelled are preferentially delivered to the distal site of cell boundaries (13, 14), consistent with polarized trafficking of PCP proteins. Noncentrosomal microtubules are aligned along the proximal–distal axis with an excess of the plus ends oriented distally prior to the onset of the PCP signaling events in the *Drosophila* wing (13, 14, 17). This suggests a mechanism whereby distinct vesicles may be trafficked in opposing orientation along polarized microtubules. An analysis of the protein composition of the Vangl2-enriched and Fzd6-enriched vesicles could provide important clues to the means by which these vesicles are directed to opposing cell-surface domains.

Materials and methods

Constructs, reagents, cell culture, immunofluorescence, and transfection

Small interference siRNAs against clathrin heavy chain or against epsinR and other clathrin adaptor subunits were purchased from Qiagen (Valencia, CA). The target sequence against clathrin heavy chain was TAATCCAATTCGAAGACCAAT. The target sequences against epsinR were CAGGCTTCGTGAAGAGCGAAA and GGTCACGAATGTTAAAAGA. The target sequence against γ1-adaptin was TAGCACAGGTTGCCACTAA and the target sequence against δ3-adaptin was CGCTGAAAATTCCTATGTT (26). The commercial antibodies were: mouse anti-Golgin 97 (Invitrogen, number A21270, RRID: AB_221447), mouse anti-GM130 (BD Biosciences, number 610823, RRID: AB_398142), mouse anti-γ1-adaptin (BD Bioscience, number 610385, RRID: AB_397768), rabbit anti-HA (Cell Signaling, number 3724, RRID: AB_1549585), sheep anti-TGN46 (AbD Serotec, number AHP500G, RRID: AB_323104), mouse anti-FLAG (Sigma, number F3165, RRID: AB_259529), rabbit anti-epsinR (Bethyl, number A301-926A, RRID: AB_1524117), rabbit anti-clathrin heavy chain (Abcam, number ab21679, RRID: AB_2083165), mouse anti-Myc (Cell Signaling, number 2276, RRID: AB_331783), goat anti-δ subunit of AP-3 (Rockland, number 600-101-290, RRID: AB_2056631), and mouse anti-α-tubulin (Abcam, number ab7291, RRID: AB_2241126).

HeLa cells and HEK293T cell lines were kindly provided by the University of California-Berkeley Cell Culture Facility and were confirmed by short tandem repeat profiling. COS-7 cells were obtained from ATCC (catalog number ATCC CRL-1651, RRID: CVCL_0224). All cell lines were tested negative for mycoplasma contamination. HeLa, HEK293T, and COS7 cells were maintained in GIBCO Dulbecco's modified Eagle's medium containing 10% fetal bovine serum (FBS), 10 milliunits/ml of penicillin, and 0.1 mg/ml of streptomycin. Transfection of siRNA or DNA constructs into HeLa cells or COS7 cells and immunofluorescence were performed as described (26). A temperature shift experiment was performed as described (26). The cycloheximide was used at the concentration of 100 μg/ml. To label surface-localized Fzd6 containing an HA tag in its extracellular N-terminal cytosolic domain, HeLa cells expressing HA-Fzd6 were incubated with the mouse anti-HA antibody (1:200) in PBS containing FBS (250 μl in 10 ml) for 40 min on ice. After several washes with PBS, cells were fixed for 15 min with 4% paraformaldehyde in PBS and then a normal immunofluorescence procedure was performed. Images were acquired with a Zeiss Axioobserver Z1 microscope system or Leica STED TCS SP5 II Confocal Laser Scanning Microscope.

The plasmid encoding p75-GFP was kindly provided by the Rodriguez-Boulan lab (Weill Cornell Medical College, New

Figure 8. A conserved polybasic motif on the Fzd6 C-terminal cytosolic domain is critical for packaging of Fzd6 into vesicles at the TGN and for Fzd6 to bind epsinR. *A,* sequence alignment of the first one-third region of Fzd6 and Frizzled3 cytosolic domain from different species indicates that the Fzd6 and Frizzled3 cytosolic domains contain a conserved polybasic motif (*red box*) and KT*XXX*W motif (*green box*). *B–G,* COS7 cells were transfected with plasmids encoding HA-Fzd6 WT (WT) (*B–D*) or the polybasic motif-deleted construct (ΔKR) (*E–G*). At day 1 after transfection, the cells were analyzed by immunofluorescence. *Scale bar*, 10 μm. *H,* TGN vesicle release reaction was performed using COS7 cells expressing HA-Fzd6 WT or HA-Fzd6 deleted of the polybasic motif (HA-Fzd6 ΔKR). *I,* quantification of the percentage of Fzd6 that was packaged into transport vesicles in TGN vesicle release reaction ($n = 4$, mean ± S.D.). *J,* a purified GST-tagged first one-third region of the Fzd6 cytosolic domain fragment (GST-Fzd6 497–567, WT) or purified GST-Fzd6 cytosolic fragment deleted of the polybasic motif (GST-Fzd6 497–567, ΔKR) were incubated with lysates from COS7 cells transfected with FLAG-tagged epsinR. After incubation the bound proteins were analyzed by immunoblot. *K,* quantification of the level of the bound epsinR normalized to the sum of the levels of epsinR bound to the WT and ΔKR mutant versions Fzd6 cytosolic domain fragments in each experiment ($n = 3$, mean ± S.D.). *L,* purified GST-Fzd6 (497–567, WT) or GST-Fzd6 (497–567, ΔKR) were incubated with purified epsinR-CHC complex. After incubation the bound proteins were analyzed by immunoblot. *M,* quantification of the level of the bound epsinR normalized to the sum of the levels of epsinR bound to the WT and ΔKR mutant versions of Fzd6 cytosolic domain fragments in each experiment ($n = 3$, mean ± S.D.).

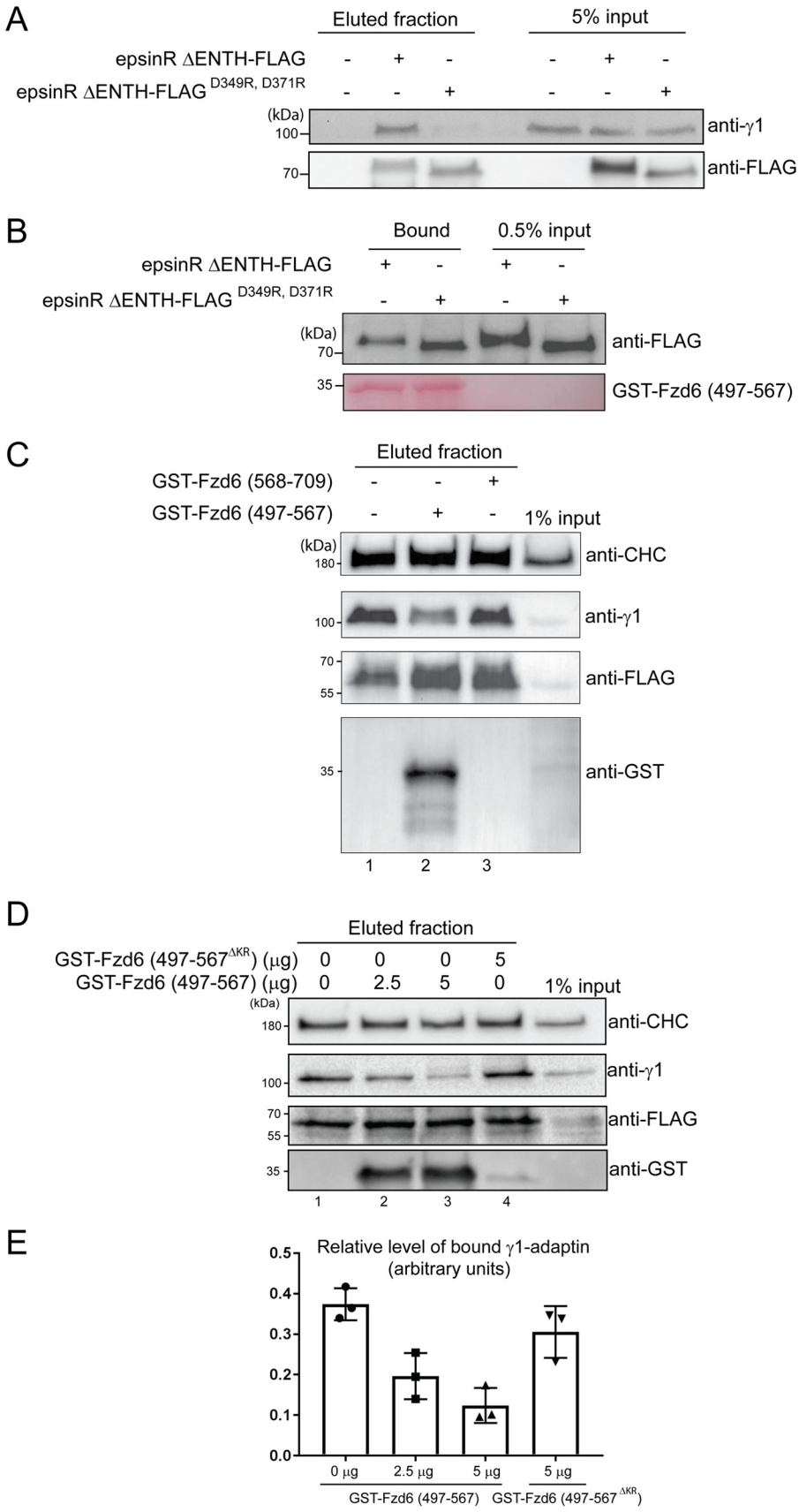
A
Eluted fraction
5% input
epsinR ΔENTH-FLAG
epsinR ΔENTH-FLAG D349R, D371R
(kDa)
100
70
anti-γ1
anti-FLAG
B
Bound
0.5% input
epsinR ΔENTH-FLAG
epsinR ΔENTH-FLAG D349R, D371R
(kDa)
70
35
anti-FLAG
GST-Fzd6 (497-567)
C
Eluted fraction
GST-Fzd6 (568-709)
GST-Fzd6 (497-567)
1% input
(kDa)
180
100
70
55
35
anti-CHC
anti-γ1
anti-FLAG
anti-GST
1 2 3
D
Eluted fraction
GST-Fzd6 (497-567ΔKR) (μg) 0 0 0 5
GST-Fzd6 (497-567) (μg) 0 2.5 5 0
1% input
(kDa)
180
100
70
55
35
anti-CHC
anti-γ1
anti-FLAG
anti-GST
1 2 3 4
E
Relative level of bound γ1-adaptin
(arbitrary units)
0.5
0.4
0.3
0.2
0.1
0.0
0 μg
2.5 μg
5 μg
5 μg
GST-Fzd6 (497-567)
GST-Fzd6 (497-567 ΔKR)

York). HA-tagged mouse Vangl2 was cloned in pCS2 (18). The plasmid encoding HA-Frizzled6 was generated by cloning full-length mouse Frizzled6 amplified from Frizzled6-Myc into pcDNA4/TO and an HA tag was inserted by PCR between Phe-22 and Thr-23. The plasmid encoding HA-Frizzled6-FLAG was generated by inserting a FLAG tag between Ser-677 and Pro-678 in HA-Frizzled6 in pcDNA4/TO. The plasmids encoding GST fusions of the Frizzled6 cytosolic fragment (aa 497–567) and the Frizzle6 cytosolic fragment (aa 568–709) were generated by cloning fragments amplified from HA-Frizzled6 into pGEX-2T. The plasmids encoding full-length epsinR, epsinR-ENTH (aa 1–166), and epsinR ΔENTH (aa 167–625) fused to FLAG and an IgG-binding ZZ domain were generated by cloning fragments amplified from human epsinR cDNA into the modified pcDNA4/TO vector encoding 3× FLAG tag and ZZ domain (kindly provided by the Zhong lab, University of Texas Southwestern, Dallas, TX).

Immunoprecipitation, protein purification, and binding assay

Immunoprecipitation of FLAG-tagged epsinR was performed by incubating 50 μl of compact anti-FLAG M2-agarose affinity beads with 10 ml of 0.5 mg/ml of cell lysates from COS7 cells transfected with epsinR-FLAG in HKT buffer (100 mM KCl, 20 mM Hepes, pH 7.2, 0.5% Triton X-100) with mixing at 4 °C overnight. After incubation, the beads were washed 4 times with 10 ml of HK buffer (100 mM KCl, 20 mM Hepes, pH 7.2) and the bound material was eluted with 1 ml of 0.2 mg/ml of FLAG peptides in HK buffer (100 mM KCl, 20 mM Hepes, pH 7.2) at 4 °C for 4 h. The eluted fraction was then dialyzed against HK buffer.

Purification of GST-tagged protein was performed as described (26). Binding assays were carried out with 4 μl of compact GSH beads bearing around 1 μg of GST-tagged Fzd6 C-terminal cytosolic domain fragments. The beads were incubated with 0.4 μg of purified epsinR-CHC complex in 400 μl of binding buffer (100 mM KCl, 20 mM Hepes, pH 7.2, 5 mM $MgCl_2$, 0.5% Triton X-100) containing 0.1 mg/ml of BSA, or incubated with 150 μl of 0.2 mg/ml of cell lysates from COS7 cells transfected with FLAG-tagged epsinR WT or truncated constructs in binding buffer at 4 °C for 90 min. After incubation, the beads were washed four times with 500 μl of binding buffer and the bound material was analyzed by immunoblot.

Vesicular release assay from the TGN

The TGN vesicular release assay was performed using COS7 cells transfected with HA-Fzd6 or HA-Vangl2. The approach was a modified version of the vesicle-budding reaction designed previously to detect COPII vesicle formation at the ER (18). Day 1 after transfection, cells grown in one 10-cm dish at around 70% confluence were incubated at 20 °C for 2 h in Opti-MEM I reduced-serum medium supplemented with 10% fetal bovine serum to accumulate newly-synthesized Fzd6 or Vangl2 at the TGN. Cells were then permeablized in 3 ml of ice-cold KOAc buffer (110 mM potassium acetate, 20 mM Hepes, pH 7.2, 2 mM magnesium acetate) containing 40 μg/ml of digitonin on ice for 5 min, and the semi-intact cells were then sedimented by centrifugation at 300 × *g* for 3 min at 4 °C. The cell pellets were resuspended in 1 ml of high salt KOAc buffer (1 M potassium acetate, 20 mM Hepes, pH 7.2, 2 mM magnesium acetate) and incubated on ice for 5 min. After incubation, permeabilized cells were washed twice with 1 ml of KOAc buffer and resuspended in 100 μl of KOAc buffer. The budding assay was performed by incubating semi-intact cells (around 0.02 OD/reaction) with 2 mg/ml of rat liver cytosol in a 100-μl reaction mixture containing 200 μM GTP and an ATP regeneration system (40 mM creatine phosphate, 0.2 mg/ml of creatine phosphokinase, and 1 mM ATP) in the presence or absence of a 0.5 μg of Sar1A(H79G) mutant protein. After incubation at 30 °C for 1 h, the reaction mixture was centrifuged at 14,000 × *g* to remove cell debris and large membranes. The medium speed supernatant was then centrifuged at 100,000 × *g* to sediment small vesicles. The pellet fraction was then analyzed by immunoblot. For density gradient flotation assay, the high speed pellet was resuspended in 100 μl of 35% OptiPrep and overlaid with 700 μl of 30% OptiPrep and 30 μl of KOAc buffer. The samples were centrifuged at 55,000 rpm in a TLS55 rotor in a Beckman ultracentrifuge for 2 h at 4 °C. After centrifugation, fractions were collected from the top to the bottom of the tube and aliquots were analyzed by SDS-PAGE and immunoblot.

To immunoisolate vesicles enriched with Vangl2 or Fzd6, the volume of the reaction mixture was scaled up to 750 μl. The medium speed supernatant was then incubated with 30 μl of compact anti-FLAG M2-agarose affinity beads at 4 °C overnight. After incubation, the beads were washed 4 times with 1 ml of KOAc buffer and eluted with 50 μl of KOAc buffer containing 0.1% Triton X-100 and 0.2 mg/ml of FLAG peptides. The eluted fraction was then analyzed by immunoblot. For immunoisolation of vesicles for the negative stain analysis, the elution buffer did not contain Triton X-100.

Figure 9. Binding of Fzd6 to epsinR causes disassociation of epsinR from AP-1. *A,* HEK293T cells were transfected with plasmids encoding a WT FLAG-tagged epsinR C terminus (epsinR ΔENTH-FLAG) or transfected with plasmids encoding an AP-1-binding deficient mutant version of FLAG-tagged epsinR C terminus (epsinR $\Delta ENTH^{D349R,D371R}$). Day 1 after transfection, FLAG-tagged epsinR constructs were immunoprecipitated and eluted by FLAG peptides and analyzed by immunoblot using the indicated antibodies. *B,* a purified GST-tagged Fzd6 cytosolic domain fragment (GST-Fzd6 497–567) was incubated with lysates from HEK293T cells transfected with plasmids encoding epsinR ΔENTH-FLAG or epsinR $\Delta ENTH^{D349R,D371R}$. After incubation the bound proteins were analyzed by immunoblot. *C,* cell lysates from HEK293T cells transfected with plasmids encoding epsinR ΔENTH-FLAG without the IgG-binding ZZ domain were incubated with M2-agarose conjugated with anti-FLAG antibodies. Subsequently, the immunoprecipitated proteins were incubated with purified GST-tagged Fzd6 cytosolic domain fragments (aa 497–567 or 568–709). After incubation, the proteins bound to M2-agarose were eluted by FLAG peptides and analyzed by immunoblot using the indicated antibodies. Data shown are a representative example of three biological repeats. *D,* cell lysates from HEK293T cells transfected with plasmids encoding epsinR without the IgG-binding ZZ domain were incubated with M2-agarose conjugated with anti-FLAG antibodies. Subsequently, the immunoprecipitated proteins were incubated with the indicated amount of a purified GST-tagged Fzd6 cytosolic domain fragment (aa 497–567, WT) or the indicated amount of a purified GST-tagged Fzd6 cytosolic domain fragment (aa 497–567, ΔKR). After incubation, the proteins bound to M2-agarose were eluted by FLAG peptides and analyzed by immunoblot using the indicated antibodies. *E,* quantification of the levels of the bound γ1-adaptin based on three independent replicates (mean ± S.D.). In each replicate of the experiment, the intensity of the bound γ1-adaptin was normalized to the sum of the intensities of the bound γ1-adaptin from all reaction conditions performed in that replicate.

Negative stain electron microscopy analysis

Carbon-coated 400-mesh copper grids were glow discharged using PELCO easiGlow™ Glow Discharge Cleaning System (Ted Pella, Inc., Redding, CA). Ten-microliters of purified and concentrated vesicle sample aliquots were air dried onto the copper grid and negatively stained for EM observation. To obtain better contrast, sample grids were post-stained with 5% uranyl acetate for 2 min and further dried before being examined using a Hitachi H-7650 transmission electron microscope with a CCD camera operating at 80 kV (Hitachi High-Technologies Corporation, Japan).

Author contributions—T. M., B. L., R. W., P. K. L., Y. H., and Y. G. data curation; T. M. and Y. G. formal analysis; T. M. and Y. G. validation; T. M., B. L., R. W., P. K. L., Y. H., and Y. G. investigation; T. M., B. L., and Y. G. visualization; L. J., R. S., and Y. G. resources; L. J., R. S., and Y. G. supervision; R. S. and Y. G. conceptualization; R. S. and Y. G. writing-review and editing; Y. G. software; Y. G. funding acquisition; Y. G. methodology; Y. G. writing-original draft; Y. G. project administration.

Acknowledgments—We thank Prof. Chris Fromme (Cornell), Prof. Karl Herrup (Hong Kong University of Science and Technology), and Prof. Jiajia Liu (Institute of Genetics and Developmental Biology, Chinese Academy of Sciences) for thoughtful discussion and comments.

References

1. Klein, T. J., and Mlodzik, M. (2005) Planar cell polarization: an emerging model points in the right direction. *Annu. Rev. Cell Dev. Biol.* **21,** 155–176 CrossRef Medline
2. Torban, E., Kor, C., and Gros, P. (2004) Van Gogh-like2 (Strabismus) and its role in planar cell polarity and convergent extension in vertebrates. *Trends Genet.* **20,** 570–577 CrossRef Medline
3. Kibar, Z., Vogan, K. J., Groulx, N., Justice, M. J., Underhill, D. A., and Gros, P. (2001) Ltap, a mammalian homolog of *Drosophila* Strabismus/Van Gogh, is altered in the mouse neural tube mutant loop-tail. *Nat. Genet.* **28,** 251–255 CrossRef Medline
4. Montcouquiol, M., and Kelley, M. W. (2003) Planar and vertical signals control cellular differentiation and patterning in the mammalian cochlea. *J. Neurosci.* **23,** 9469–9478 CrossRef Medline
5. Henderson, D. J., Phillips, H. M., and Chaudhry, B. (2006) Vang-like 2 and noncanonical Wnt signaling in outflow tract development. *Trends Cardiovasc. Med.* **16,** 38–45 CrossRef Medline
6. Fröjmark, A. S., Schuster, J., Sobol, M., Entesarian, M., Kilander, M. B., Gabrikova, D., Nawaz, S., Baig, S. M., Schulte, G., Klar, J., and Dahl, N. (2011) Mutations in Frizzled 6 cause isolated autosomal-recessive nail dysplasia. *Am. J. Hum. Genet.* **88,** 852–860 CrossRef Medline
7. Guo, N., Hawkins, C., and Nathans, J. (2004) Frizzled6 controls hair patterning in mice. *Proc. Natl. Acad. Sci. U.S.A.* **101,** 9277–9281 CrossRef Medline
8. Wang, Y., Guo, N., and Nathans, J. (2006) The role of Frizzled3 and Frizzled6 in neural tube closure and in the planar polarity of inner-ear sensory hair cells. *J. Neurosci.* **26,** 2147–2156 CrossRef Medline
9. Devenport, D. (2014) The cell biology of planar cell polarity. *J. Cell Biol.* **207,** 171–179 CrossRef Medline
10. Chen, W. S., Antic, D., Matis, M., Logan, C. Y., Povelones, M., Anderson, G. A., Nusse, R., and Axelrod, J. D. (2008) Asymmetric homotypic interactions of the atypical cadherin flamingo mediate intercellular polarity signaling. *Cell* **133,** 1093–1105 CrossRef Medline
11. Wu, J., Roman, A. C., Carvajal-Gonzalez, J. M., and Mlodzik, M. (2013) Wg and Wnt4 provide long-range directional input to planar cell polarity orientation in *Drosophila*. *Nat. Cell Biol.* **15,** 1045–1055 CrossRef Medline
12. Bayly, R., and Axelrod, J. D. (2011) Pointing in the right direction: new developments in the field of planar cell polarity. *Nat. Rev. Genet.* **12,** 385–391 CrossRef Medline
13. Shimada, Y., Yonemura, S., Ohkura, H., Strutt, D., and Uemura, T. (2006) Polarized transport of Frizzled along the planar microtubule arrays in *Drosophila* wing epithelium. *Dev. Cell* **10,** 209–222 CrossRef Medline
14. Olofsson, J., Sharp, K. A., Matis, M., Cho, B., and Axelrod, J. D. (2014) Prickle/spiny-legs isoforms control the polarity of the apical microtubule network in planar cell polarity. *Development* **141,** 2866–2874 CrossRef Medline
15. Peng, Y., and Axelrod, J. D. (2012) Asymmetric protein localization in planar cell polarity: mechanisms, puzzles, and challenges. *Curr. Top. Dev. Biol.* **101,** 33–53 CrossRef Medline
16. Yang, Y., and Mlodzik, M. (2015) Wnt-Frizzled/planar cell polarity signaling: cellular orientation by facing the wind (Wnt). *Annu. Rev. Cell Dev. Biol.* **31,** 623–646 CrossRef Medline
17. Harumoto, T., Ito, M., Shimada, Y., Kobayashi, T. J., Ueda, H. R., Lu, B., and Uemura, T. (2010) Atypical cadherins Dachsous and Fat control dynamics of noncentrosomal microtubules in planar cell polarity. *Dev. Cell* **19,** 389–401 CrossRef Medline
18. Merte, J., Jensen, D., Wright, K., Sarsfield, S., Wang, Y., Schekman, R., and Ginty, D. D. (2010) Sec24b selectively sorts Vangl2 to regulate planar cell polarity during neural tube closure. *Nat. Cell Biol.* **12,** 41–46; sup pp 1–8 CrossRef Medline
19. Guo, Y., Sirkis, D. W., and Schekman, R. (2014) Protein sorting at the trans-Golgi network. *Annu. Rev. Cell Dev. Biol.* **30,** 169–206 CrossRef Medline
20. Donaldson, J. G., and Jackson, C. L. (2011) ARF family G proteins and their regulators: roles in membrane transport, development and disease. *Nat. Rev. Mol. Cell Biol.* **12,** 362–375 CrossRef Medline
21. Gillingham, A. K., and Munro, S. (2007) The small G proteins of the Arf family and their regulators. *Annu. Rev. Cell Dev. Biol.* **23,** 579–611 CrossRef Medline
22. Curwin, A. J., von Blume, J., and Malhotra, V. (2012) Cofilin-mediated sorting and export of specific cargo from the Golgi apparatus in yeast. *Mol. Biol. Cell* **23,** 2327–2338 CrossRef Medline
23. von Blume, J., Alleaume, A. M., Cantero-Recasens, G., Curwin, A., Carreras-Sureda, A., Zimmermann, T., van Galen, J., Wakana, Y., Valverde, M. A., and Malhotra, V. (2011) ADF/cofilin regulates secretory cargo sorting at the TGN via the Ca^{2+} ATPase SPCA1. *Dev. Cell* **20,** 652–662 CrossRef Medline
24. von Blume, J., Duran, J. M., Forlanelli, E., Alleaume, A. M., Egorov, M., Polishchuk, R., Molina, H., and Malhotra, V. (2009) Actin remodeling by ADF/cofilin is required for cargo sorting at the trans-Golgi network. *J. Cell Biol.* **187,** 1055–1069 CrossRef Medline
25. Kienzle, C., Basnet, N., Crevenna, A. H., Beck, G., Habermann, B., Mizuno, N., and von Blume, J. (2014) Cofilin recruits F-actin to SPCA1 and promotes Ca^{2+}-mediated secretory cargo sorting. *J. Cell Biol.* **206,** 635–654 CrossRef Medline
26. Guo, Y., Zanetti, G., and Schekman, R. (2013) A novel GTP-binding protein-adaptor protein complex responsible for export of Vangl2 from the trans Golgi network. *Elife* **2,** e00160 Medline
27. Wakana, Y., van Galen, J., Meissner, F., Scarpa, M., Polishchuk, R. S., Mann, M., and Malhotra, V. (2012) A new class of carriers that transport selective cargo from the trans Golgi network to the cell surface. *EMBO J.* **31,** 3976–3990 CrossRef Medline
28. Ponnambalam, S., Girotti, M., Yaspo, M. L., Owen, C. E., Perry, A. C., Suganuma, T., Nilsson, T., Fried, M., Banting, G., and Warren, G. (1996) Primate homologues of rat TGN38: primary structure, expression and functional implications. *J. Cell Sci.* **109,** 675–685 Medline
29. Miller, E. A., Beilharz, T. H., Malkus, P. N., Lee, M. C., Hamamoto, S., Orci, L., and Schekman, R. (2003) Multiple cargo binding sites on the COPII subunit Sec24p ensure capture of diverse membrane proteins into transport vesicles. *Cell* **114,** 497–509 CrossRef Medline
30. Deborde, S., Perret, E., Gravotta, D., Deora, A., Salvarezza, S., Schreiner, R., and Rodriguez-Boulan, E. (2008) Clathrin is a key regulator of basolateral polarity. *Nature* **452,** 719–723 CrossRef Medline

31. Mills, I. G., Praefcke, G. J., Vallis, Y., Peter, B. J., Olesen, L. E., Gallop, J. L., Butler, P. J., Evans, P. R., and McMahon, H. T. (2003) EpsinR: an AP1/clathrin interacting protein involved in vesicle trafficking. *J. Cell Biol.* **160,** 213–222 CrossRef Medline
32. Carvajal-Gonzalez, J. M., Balmer, S., Mendoza, M., Dussert, A., Collu, G., Roman, A. C., Weber, U., Ciruna, B., and Mlodzik, M. (2015) The clathrin adaptor AP-1 complex and Arf1 regulate planar cell polarity *in vivo*. *Nat. Commun.* **6,** 6751 CrossRef Medline
33. Lee, J. H., Overstreet, E., Fitch, E., Fleenor, S., and Fischer, J. A. (2009) *Drosophila* liquid facets-Related encodes Golgi epsin and is an essential gene required for cell proliferation, growth, and patterning. *Dev. Biol.* **331,** 1–13 CrossRef Medline
34. Leventis, P. A., Da Sylva, T. R., Rajwans, N., Wasiak, S., McPherson, P. S., and Boulianne, G. L. (2011) Liquid facets-related (lqfR) is required for egg chamber morphogenesis during *Drosophila* oogenesis. *PLoS ONE* **6,** e25466 CrossRef Medline
35. Lee, J. H., and Fischer, J. A. (2012) Drosophila Tel2 is expressed as a translational fusion with EpsinR and is a regulator of wingless signaling. *PLoS ONE* **7,** e46357 CrossRef Medline
36. Dodd, M. E., Hatzold, J., Mathias, J. R., Walters, K. B., Bennin, D. A., Rhodes, J., Kanki, J. P., Look, A. T., Hammerschmidt, M., and Huttenlocher, A. (2009) The ENTH domain protein Clint1 is required for epidermal homeostasis in zebrafish. *Development* **136,** 2591–2600 CrossRef Medline
37. Sonawane, M., Carpio, Y., Geisler, R., Schwarz, H., Maischein, H. M., and Nuesslein-Volhard, C. (2005) Zebrafish penner/lethal giant larvae 2 functions in hemidesmosome formation, maintenance of cellular morphology and growth regulation in the developing basal epidermis. *Development* **132,** 3255–3265 CrossRef Medline
38. Aguilar, R. C., Longhi, S. A., Shaw, J. D., Yeh, L. Y., Kim, S., Schön, A., Freire, E., Hsu, A., McCormick, W. K., Watson, H. A., and Wendland, B. (2006) Epsin N-terminal homology domains perform an essential function regulating Cdc42 through binding Cdc42 GTPase-activating proteins. *Proc. Natl. Acad. Sci. U.S.A.* **103,** 4116–4121 CrossRef Medline
39. Saint-Pol, A., Yélamos, B., Amessou, M., Mills, I. G., Dugast, M., Tenza, D., Schu, P., Antony, C., McMahon, H. T., Lamaze, C., and Johannes, L. (2004) Clathrin adaptor epsinR is required for retrograde sorting on early endosomal membranes. *Dev. Cell* **6,** 525–538 CrossRef Medline
40. Chidambaram, S., Müllers, N., Wiederhold, K., Haucke, V., and von Mollard, G. F. (2004) Specific interaction between SNAREs and epsin N-terminal homology (ENTH) domains of epsin-related proteins in trans-Golgi network to endosome transport. *J. Biol. Chem.* **279,** 4175–4179 CrossRef Medline
41. Chidambaram, S., Zimmermann, J., and von Mollard, G. F. (2008) ENTH domain proteins are cargo adaptors for multiple SNARE proteins at the TGN endosome. *J. Cell Sci.* **121,** 329–338 CrossRef Medline
42. Hirst, J., Miller, S. E., Taylor, M. J., von Mollard, G. F., and Robinson, M. S. (2004) EpsinR is an adaptor for the SNARE protein Vti1b. *Mol. Biol. Cell* **15,** 5593–5602 CrossRef Medline
43. Miller, S. E., Collins, B. M., McCoy, A. J., Robinson, M. S., and Owen, D. J. (2007) A SNARE-adaptor interaction is a new mode of cargo recognition in clathrin-coated vesicles. *Nature* **450,** 570–574 CrossRef Medline
44. Wang, J., Gossing, M., Fang, P., Zimmermann, J., Li, X., von Mollard, G. F., Niu, L., and Teng, M. (2011) Epsin N-terminal homology domains bind on opposite sides of two SNAREs. *Proc. Natl. Acad. Sci. U.S.A.* **108,** 12277–12282 CrossRef Medline
45. Owen, D. J., Collins, B. M., and Evans, P. R. (2004) Adaptors for clathrin coats: structure and function. *Annu. Rev. Cell Dev. Biol.* **20,** 153–191 CrossRef Medline
46. Horvath, C. A., Vanden Broeck, D., Boulet, G. A., Bogers, J., and De Wolf, M. J. (2007) Epsin: inducing membrane curvature. *Int. J. Biochem. Cell Biol.* **39,** 1765–1770 CrossRef Medline
47. Hawryluk, M. J., Keyel, P. A., Mishra, S. K., Watkins, S. C., Heuser, J. E., and Traub, L. M. (2006) Epsin 1 is a polyubiquitin-selective clathrin-associated sorting protein. *Traffic* **7,** 262–281 CrossRef Medline
48. Barriere, H., Nemes, C., Lechardeur, D., Khan-Mohammad, M., Fruh, K., and Lukacs, G. L. (2006) Molecular basis of oligoubiquitin-dependent internalization of membrane proteins in mammalian cells. *Traffic* **7,** 282–297 CrossRef Medline
49. Pryor, P. R., Jackson, L., Gray, S. R., Edeling, M. A., Thompson, A., Sanderson, C. M., Evans, P. R., Owen, D. J., and Luzio, J. P. (2008) Molecular basis for the sorting of the SNARE VAMP7 into endocytic clathrin-coated vesicles by the ArfGAP Hrb. *Cell* **134,** 817–827 CrossRef Medline
50. Shukla, A. K., Westfield, G. H., Xiao, K., Reis, R. I., Huang, L. Y., Tripathi-Shukla, P., Qian, J., Li, S., Blanc, A., Oleskie, A. N., Dosey, A. M., Su, M., Liang, C. R., Gu, L. L., Shan, J. M., *et al.* (2014) Visualization of arrestin recruitment by a G-protein-coupled receptor. *Nature* **512,** 218–222 CrossRef Medline
51. Parmar, H. B., Barry, C., and Duncan, R. (2014) Polybasic trafficking signal mediates Golgi export, ER retention or ER export and retrieval based on membrane-proximity. *PLoS ONE* **9,** e94194 CrossRef Medline
52. Parmar, H. B., Barry, C., Kai, F., and Duncan, R. (2014) Golgi complex-plasma membrane trafficking directed by an autonomous, tribasic Golgi export signal. *Mol. Biol. Cell* **25,** 866–878 CrossRef Medline
53. Parmar, H. B., and Duncan, R. (2016) A novel tribasic Golgi export signal directs cargo protein interaction with activated Rab11 and AP-1-dependent Golgi-plasma membrane trafficking. *Mol. Biol. Cell* **27,** 1320–1331 CrossRef Medline
54. Copic, A., Starr, T. L., and Schekman, R. (2007) Ent3p and Ent5p exhibit cargo-specific functions in trafficking proteins between the trans-Golgi network and the endosomes in yeast. *Mol. Biol. Cell* **18,** 1803–1815 CrossRef Medline
55. Hirst, J., Edgar, J. R., Borner, G. H., Li, S., Sahlender, D. A., Antrobus, R., and Robinson, M. S. (2015) Contributions of epsinR and gadkin to clathrin-mediated intracellular trafficking. *Mol. Biol. Cell* **26,** 3085–3103 CrossRef Medline
56. Hirst, J., Motley, A., Harasaki, K., Peak Chew, S. Y., and Robinson, M. S. (2003) EpsinR: an ENTH domain-containing protein that interacts with AP-1. *Mol. Biol. Cell* **14,** 625–641 CrossRef Medline